

8128

NATIONAL LIBRARY
OTTAWA



BIBLIOTHÈQUE NATIONALE
OTTAWA

NAME OF AUTHOR... JOHN CHARLES WOOD TAYLOR...
 TITLE OF THESIS... LUMINESCENCE AND EXCITONS
 ... IN CUPROUS OXIDE ...
 UNIVERSITY... UNIVERSITY OF ALBERTA ...
 DEGREE FOR WHICH THESIS WAS PRESENTED... DOCTOR OF PHILOSOPHY
 YEAR THIS DEGREE GRANTED... 1971 ...

Permission is hereby granted to THE NATIONAL LIBRARY
 OF CANADA to microfilm this thesis and to lend or sell copies
 of the film.

The author reserves other publication rights, and
 neither the thesis nor extensive extracts from it may be
 printed or otherwise reproduced without the author's
 written permission.

(Signed).... John Taylor....

PERMANENT ADDRESS:

..... 9611-105 St.
 EDMONTON

DATED..... 18/Nov 1970

THE UNIVERSITY OF ALBERTA

LUMINESCENCE AND EXCITONS IN CUPROUS OXIDE

BY



JOHN CHARLES WOOD TAYLOR

A THESIS

SUBMITTED TO THE FACULTY OF GRADUATE STUDIES IN
PARTIAL FULFILMENT OF THE REQUIREMENTS FOR THE
DEGREE OF DOCTOR OF PHILOSOPHY

DEPARTMENT OF PHYSICS

EDMONTON, ALBERTA

SPRING, 1971

UNIVERSITY OF ALBERTA
FACULTY OF GRADUATE STUDIES

The undersigned certify that they have read,
and recommend to the Faculty of Graduate Studies for
acceptance, a thesis entitled "LUMINESCENCE AND EXCITONS
IN CUPROUS OXIDE", submitted by John Charles Wood Taylor
in partial fulfilment of the requirements for the degree
of Doctor of Philosophy.

Frank H. Weirha
Supervisor

A. Steiner

R. E. Meloy

J. B. ...

Baldemar Di Bartolo
External Examiner

Date 12/Mar/70

ABSTRACT.

In this thesis, the results of a detailed study on the 1 μ infrared luminescence in Cu₂O after optical excitation are reported. It was found that the luminescence was an extrinsic property of the material, and, by making measurements of the optical excitation curves, it was shown that the luminescence was intimately connected with the exciton states of the bulk material. It was then possible to set up a model in which the observed luminescence was the radiative decay of an exciton captured by the extrinsic entity in the lattice (ie. the luminescent center), and on the basis of this model, several properties of the excitons themselves could be measured.

In this way, it was found that only n=1 excitons were responsible for luminescence and a good agreement was obtained between luminescence results and Elliott's theory of the n=2 exciton (yellow series) absorption line asymmetry.

On investigating a size effect in luminescence excitation curves with decreasing sample thickness, it was further shown that the luminescence was associated with not only the n=1 exciton of the yellow series, but with the n=1 of the green series also.

A quantity ϕ proportional to the capture cross-section for these excitons by the luminescent center was derived, and from structure in curves of ϕ versus incident light energy, it was possible to determine the $\underline{K} = 0$ energy of the green series $n=1$ excitons.

Proceeding on the basis of the model whereby only $n=1$ excitons (of either series) are responsible for luminescence, a value for the fraction of $n=2$ excitons (yellow series) which decay to $n=1$ excitons (yellow series) is derived from measurements of the $n=2$ exciton structure in luminescence excitation curves.

An attempt to identify the luminescent center using the technique of electron paramagnetic resonance was unsuccessful, although some interesting results were obtained.

In an investigation into the phonon spectra of the material, a complex Raman spectrum was measured using the Krypton laser line at $6471\overset{\circ}{\text{A}}$.

ACKNOWLEDGEMENTS.

It is a particular pleasure to thank Dr. F.L. Weichman for initially suggesting the research problem and for his help and encouragement during the course of the work.

My thanks are also due to Dr. R.E.D. McClung of the Chemistry department for his interest and assistance during the e.p.r. investigation, which was carried out using his apparatus.

The assistance of Dr. J.E. Bertie of the Chemistry department in kindly allowing the use of the Raman and Infrared absorption equipment is also gratefully acknowledged.

It is a great pleasure to thank the technical staff of the Physics department and, in particular, Mr. H. McClung and Mr. N. Riebeek, for their unstinting assistance during all stages of the work.

My thanks are also due to Mr. G. Bigam of the Chemistry department for the design and construction of the e.p.r. cryostat.

I would like to thank the Physics department for financial support in the form of teaching assistantships during my stay in the department and, further, for the provision of an atmosphere which I

personally have found conducive to work in experimental physics.

I must also express my appreciation to Randy K. Lomnes for his help in setting up the computation programs and for his contribution to our many valuable discussions.

Finally, my sincere thanks are due to my wife, Jennifer, for her continued encouragement during the course of this work and for her help in reading and typing the manuscript.

J.C.W.T.

For
Jennifer and Jeremy

And
My Parents,
Margaret and Samuel

TABLE OF CONTENTS

	<u>PAGE</u>
Chapter 1 : Introduction	1
Chapter 2 : Early Experimental Results	6
Chapter 3 : Excitation Spectra for Luminescence	18
Chapter 4 : Band Structure and Absorption Processes	27
Chapter 5 : Luminescence Excitation Processes and the Exciton Line Shape Problem	36
Chapter 6 : Thickness Dependence and Exciton Structure	43
Chapter 7 : Exciton Size Effect in Luminescence	62
Chapter 8 : The Luminescent Center and Electron Paramagnetic Resonance	70
Chapter 9 : Conclusion	86
 Addendum : Raman Effect in Cuprous Oxide Compared to Infrared Absorption	
Introduction	92
Experiment	93
Discussion	98
Conclusion	104

Appendix A	:	The Electron-Photon Interaction	<u>PAGE</u> <u>106</u>
Appendix B	:	A.P.L. Programs and Routines	113
Bibliography			118

LIST OF FIGURES

	<u>PAGE</u>
Figure 1 : The emission spectrum of Cu_2O after optical excitation	9
Figure 2 : Temperature dependence of the luminescence	10
Figure 3 : A plot of $\log \left(\frac{1}{L^2} \frac{dL}{d\beta} \right)$ vs. β	12
Figure 4 : Luminescence intensity dependence on intensity of incident light	14
Figure 5 : Argon flash tube design	16
Figure 6 : Cryostat for measuring luminescence	19
Figure 7 : Luminescence excitation curves for a strongly emitting sample	21
Figure 8 : Luminescence excitation curve for a weakly emitting sample	23
Figure 9 : Photoconductivity excitation curve for a strongly emitting sample	26
Figure 10 : The band structure of Cu_2O	28
Figure 11 : Direct and Indirect transitions as they appear on the band scheme	30
Figure 12 : Absorption curve for Cu_2O	32
Figure 13 : A detail of the luminescence excitation curve of Fig.8 in the region of $n=2$	40
Figure 14 : Schematic of the liquid N_2 cryostat	45
Figure 15 : Luminescence excitation curves for a weakly emitting sample for the three	

	<u>PAGE</u>
thicknesses a) 0.1 cm b) 0.0045 cm and c) 0.003 cm at 77°K	46
Figure 16 : A simplified absorption curve for Cu ₂ O	48
Figure 17 : Diagram for sample illumination and detection arrangement	51
Figure 18 : A plot of ϕ versus incident light energy for four sample thicknesses	54
Figure 19 : Approximate dispersion curves for excitons	56
Figure 20 : Model for excitation and decay processes for the n=2 exciton of the yellow series	63
Figure 21 : Plot of the ratio $w_2:w_{21}$ for various sample thicknesses required to produce a smooth curve in luminescence	67
Figure 22 : Calculated luminescence excitation curve	68
Figure 23 : The e.p.r. Helium cryostat	73
Figure 24 : Plot of $\log_{10}\sigma$ vs. $1/T$	75
Figure 25 : Photoconductivity excitation curves for samples A,B,C,D,E, and F at 300°K	76
Figure 26 : Luminescence excitation curves for samples A,B,D,E, and F at 77°K	77
Figure 27 : Electron paramagnetic resonance for Cu ₂ O at 4.2°K	81

	<u>PAGE</u>
Figure 28 : Plots of ϕ vs. λ for the samples A,B,D,E, and F of Fig.26	89
Figure 29 : The Raman spectrum of Cu_2O	96
Figure 30 : Infrared transmission curve for Cu_2O	99

LIST OF TABLES

	<u>PAGE</u>
Table 1 : Summary of sample treatment history, activation energies, photoconductivity and luminescence properties for samples A,B,C,D,E, and F	78
Table 2 : Summary of Raman and Infrared results	95
Table 3 : Known combination bands in Cu_2O	102

CHAPTER 1.

Introduction.

In recent years, there has been a critical re-evaluation of earlier work on Cu_2O . There are several reasons for this, the most important, however, being the recent improvements in sample preparation and handling techniques by most workers in the field, which allow single crystals to be used and reliable measurements to be made. It was found that for properties such as electrical conductivity, activation energy, and photoconductivity, discrepancies existed between the older and more recent results (see for example Fortin and Weichman (1962) and Weichman and Kuzel (1970)).

With this trend towards the repetition of earlier experiments on the physical properties of Cu_2O in mind, we felt that a detailed study should be made of the infrared luminescence of the material after optical excitation. This luminescence was first reported by Seibt (1939) and has since been studied by Lashkarev and Kossonogova (1946), Karkhanin (1952), Grillot (1956), Bloem et al. (1956), Tolstoi (1957), Bloem (1958), Pastrnyak (1961), Vorob'ev and Karkhanin

(1961), Gorban et al. (1961), Tolstoi and Abramov (1968), and Gross and Kreingold (1968).

These references are listed in chronological order and constitute the bulk of the available material dealing with the infrared luminescence after optical excitation.

It was found by these authors that a strong luminescence at 1μ could be observed, with a quantum efficiency as high as 10% at room temperature. Emission at shorter wavelengths of 0.7 and 0.8μ was also reported by Bloem et al. (1956), although no evidence of these lines was seen for our samples in the present work.

The first serious attempt at setting up a model for luminescence was made by Tolstoi (1957) from measurements of the temperature dependence of the emitted light intensity. He concluded that the most probable mechanism was a radiative decay from an exciton state.

Although we show here that the temperature dependence for our samples can be explained on a different model, Tolstoi's concept of an exciton decay was adopted by Pastrnyak (1961) when he published the first luminescence excitation spectrum. This spectrum contained little detail, but did show that the

luminescence could be excited by visible light of all wavelengths up to a cut-off value of about 0.63μ . The only detailed excitation spectrum published up to the present work was by Gross and Kreingold (1968) whose curve shows a sharp peak at 0.6μ at 77°K , with a cut-off at 0.62μ in agreement with the work of Pastrnyak. Gross and Kreingold also interpret their excitation curve to be to exciton states but since they observe several sharp peaks unobserved by us or other workers, which they also attribute to exciton effects, no conclusive deductions can be made as to which exciton levels are involved.

It was therefore felt that the present work should be directed towards measuring at different temperatures the excitation spectra for a number of samples prepared under a variety of conditions. Further, in order to better understand the electronic processes involved for luminescence, a comparison with other physical properties such as electrical conductivity, activation energy, optical absorption and electron paramagnetic resonance was also made.

In the course of our work we were able to show that the luminescence is indeed strongly associated with the exciton states and known absorption processes of the material. The luminescence is, in fact, so

sensitive to excitons that the presence of the previously unobserved $n=1$ exciton of the green series was detected and an experimental verification was made of the theory of the $n=2$ exciton line asymmetry problem by Elliott (1959), (1960).

The investigation into the luminescent properties also led us further afield, and the first experimental observation of electron paramagnetic resonance (e.p.r.) in Cu_2O was obtained for some of our samples, in an unsuccessful attempt to determine the nature of the center responsible for the luminescence. (Note : A resonance has been reported by O'Keefe et al. (1963) for neutron irradiated samples only, although no spectrum was published.) In a similar way, one of the first reported Raman spectra for Cu_2O was observed in an investigation into the phonon spectra of the material.

Since the Raman effect has little to do with the luminescence results, it will be briefly discussed in an addendum to the main sections of the thesis.

For the sake of readability and continuity of discussion, the general background theory of optical absorption has also been relegated to an appendix.

References to sources of more general theories of luminescence than those developed here are given in

the text. Also, a theory for photoconduction in Cu_2O for samples prepared in this laboratory has been fully developed by Fortin (1965) and no attempt will be made here to duplicate this work.

CHAPTER 2.

Early Experimental Results.

In a series of preliminary experiments, several general characteristics of the luminescence were observed. It was seen that the luminescent intensity varied strongly from sample to sample and this was attributed to slight differences in either the oxidation or annealing process during sample preparation, since most of the variation in optical and electrical properties can be traced to the degree of non-stoichiometry from the ideal Cu_2O lattice.

Some samples were then prepared, during an investigation into the effects of preparation conditions, which luminesced strongly even at room temperature. The maximum quantum efficiency for these samples at 300°K for incident radiation at the wavelength of peak response was found to be as high as 5% increasing by a factor of 4 or 5 at 4.2°K .

The quantum efficiency η is simply defined by

$$\eta = \frac{L}{I} \quad 1)$$

where L is the total number of luminescent photons

emitted per unit time and I is the total number of photons of exciting radiation entering at the surface of the sample.

The preparation conditions giving rise to this strong luminescence were produced by oxidising for a short time and then allowing the sample to cool under a vacuum of 10^{-4} torr from a temperature of 1100°C . It was then found that the luminescence of such a sample could be reduced in intensity by three or four orders of magnitude by re-heating to 1100°C for one hour and allowing to cool under a vacuum of 10^{-7} torr. These results are in complete contrast to those found in a later, more detailed investigation, where it was seen that samples cooled from 1000°C under good vacuum ($\sim 10^{-7}$ torr) were better emitters than those cooled from the same temperature at a lower vacuum ($\sim 10^{-4}$ torr). The disagreement was resolved, however, when it was found that samples which were originally poor emitters could be made to luminesce strongly if a piece of copper metal was introduced into the high temperature treatment system and the sample then allowed to cool under a vacuum of 10^{-7} torr.

The misleading results found above are thus due to the presence of unoxidised copper in the samples due to the short oxidation time. This copper is

responsible for the strong luminescence which disappears on re-heating to 1000°C due to the removal of the surplus.

The spectral distribution of the luminescence was measured for a number of samples using a two monochromator system. The luminescent intensity versus emission wavelength curve is a single bell-shaped peak at 1μ with a half width of 1000Å . The curve for illumination by a 2mw He-Ne laser is shown in Fig.1 for a sample temperature of 300°K. No shift in peak position was observed with change in exciting wavelength or change in temperature. No luminescence was detected at wavelengths of 0.7 and 0.8 μ as mentioned earlier, although a careful search was made. (Note : A weak emission in the red, peaked at about 0.65 μ , was observed for some of our samples in electroluminescence.)

The temperature dependence of the luminescent intensity for constant incident wavelength was measured for a number of samples and the luminescence was seen to increase strongly with decreasing temperature, Fig.2. An attempt was made to fit the luminescence versus temperature curves (for the incident wavelength of maximum response) to standard models for luminescence.

A good fit was however obtained only for a

Figure 1 : The emission spectrum of Cu_2O after optical excitation by a 2 mw He-Ne laser at 0.6328μ . The temperature of measurement is 300°K .

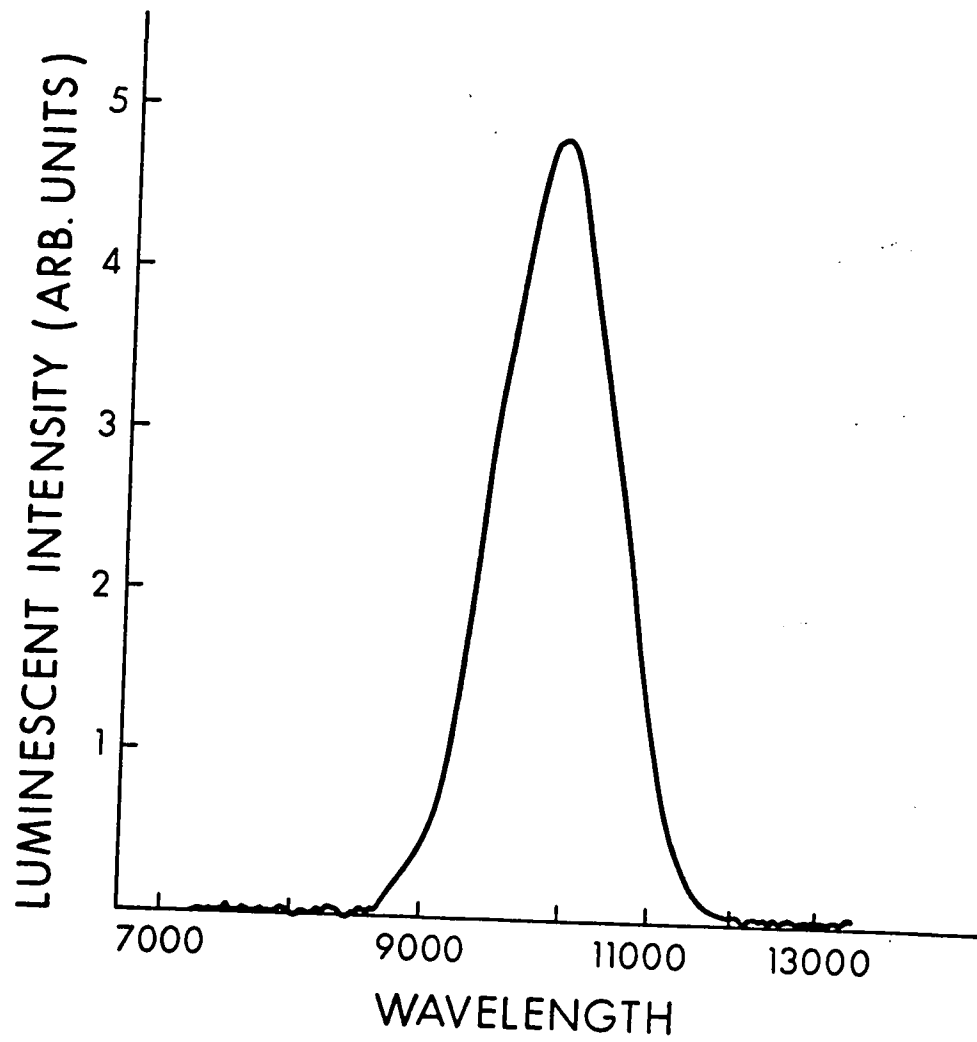
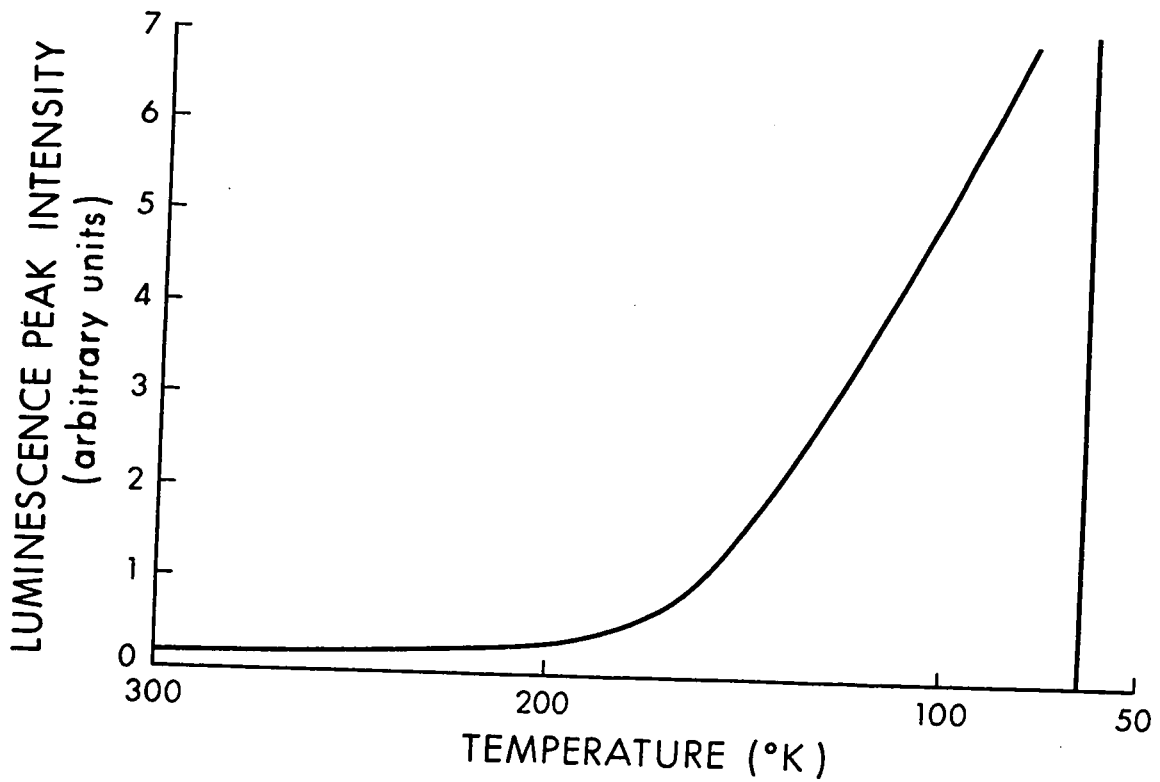


Figure 2 : Temperature dependence of the luminescence peak intensity in the range 300 to 77°K.



model in which the population of the lower level of a two level luminescence system varied with temperature. The expression for luminescence was given by

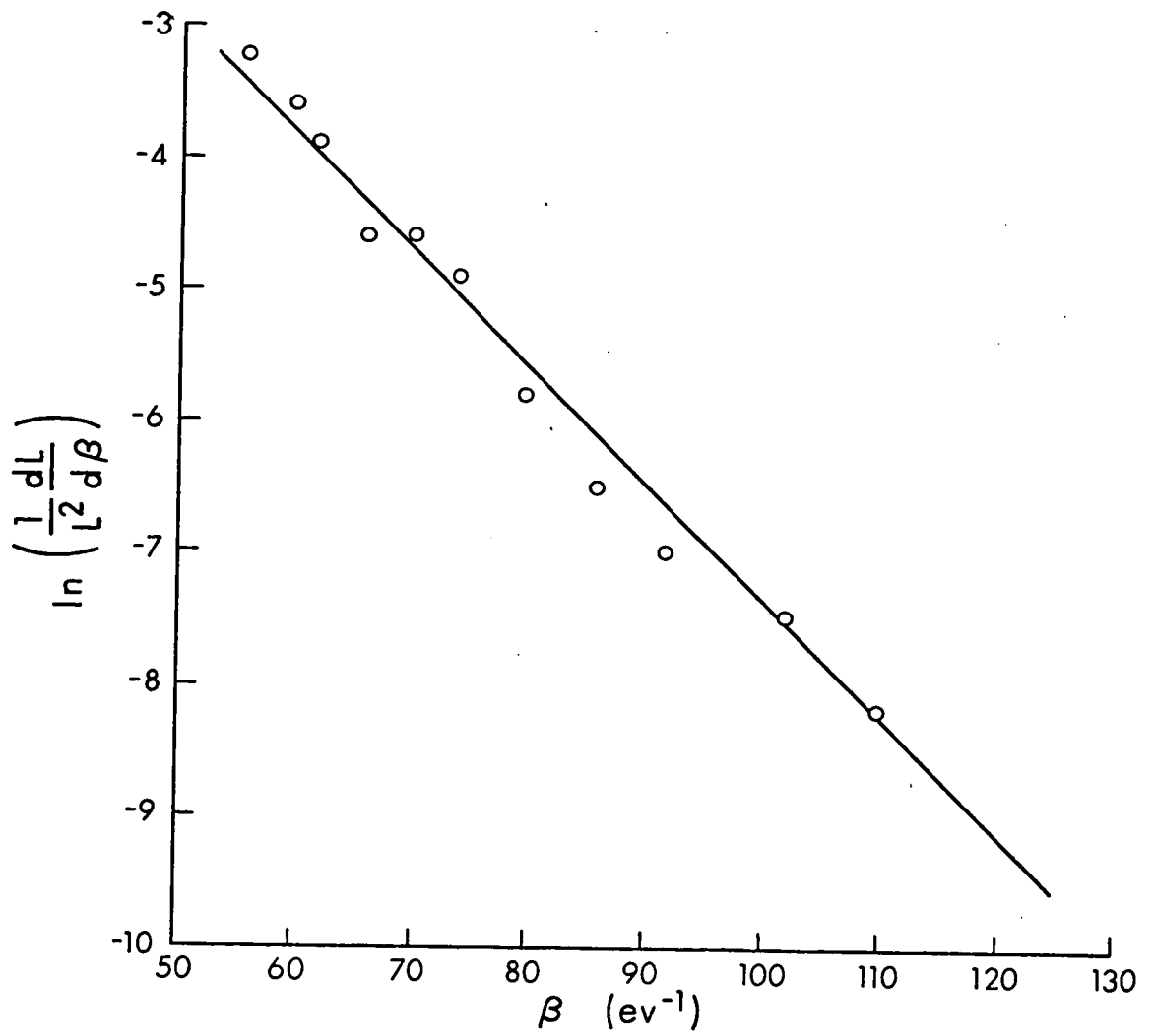
$$L \propto N_e (1 - f(E')) \quad 2)$$

where L is the number of luminescent photons emitted per unit time, N_e is the number of excited states assumed here to be constant with constant intensity of incident light, $f(E')$ is the fermi distribution function which determines the population of the lower level in the luminescent transition, and E' is the energy of this lower state relative to the fermi level.

Thus a plot of $\log \left(\frac{1}{L} \frac{dL}{d\beta} \right)$ versus β , where $\beta = kT$, should give a straight line graph whose slope equals $-E'$. A plot of the experimental results is shown in Fig.3. A straight line is obtained with $E' = 0.1$ eV, indicating that expression 2) is a good approximation in the temperature range chosen.† At lower temperatures, expression 2) would be expected to be invalid when the occupation of the lower state is predominantly determined by the luminescent decay rather than by thermal excitation. Furthermore, the assumption made that any variation of N_e with temperature is small compared to the variation of $f(E')$,

†300 to 77°K

Figure 3 : A plot of $\log \left(\frac{1}{L^2} \frac{dL}{d\beta} \right)$ vs. β .
The slope of the straight line is $-E'$.

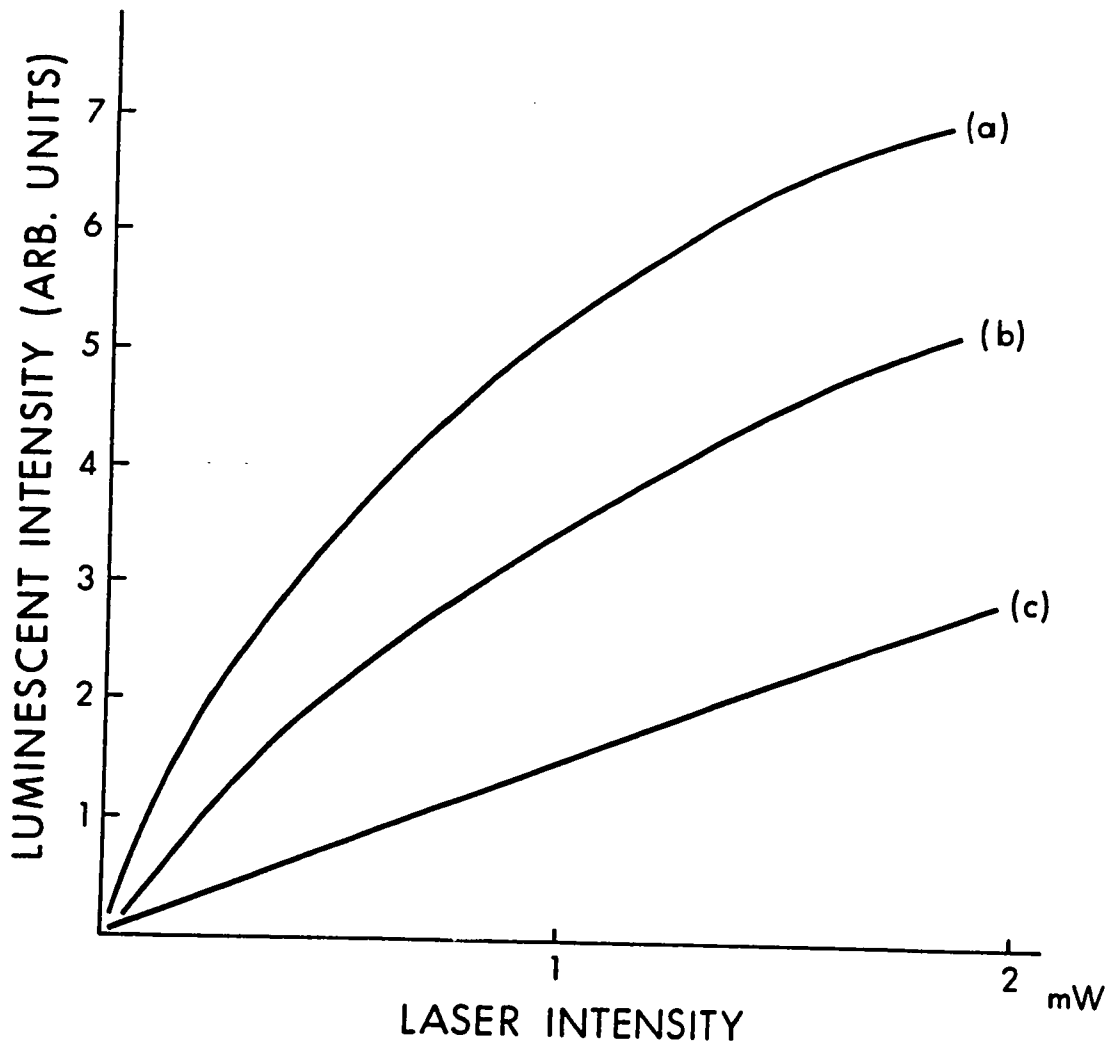


appears to be valid.

The luminescent intensity had been found by Tolstoi and Abramov (1967) to be non linear with varying incident light intensity for a luminescent line at 0.93μ . This effect was investigated for our samples using a 2mw He-Ne laser as incident light source. At 300°K this is permissible since there remains some optical absorption at the laser wavelength of 0.6328μ .

Two approaches are possible which are not necessarily equivalent : (1) the intensity of the incident light can be varied while maintaining a constant area of illumination on the sample, and (2) the intensity of the incident light may be kept constant and the illuminated area of the sample varied by focussing or de-focussing the laser beam by changing the position of a simple lens. The results for varying incident light intensity with three different sizes of illuminated area are shown in Fig.4. Process (1) is therefore represented by curves (a), (b) and (c), process (2) would be represented by going vertically from curve to curve. The non-linearity therefore appears when the photon flux is a maximum, whether this is produced by increases in light intensity or reduction in illumination area. Processes (1) and (2) therefore produce identical results in this case. The

Figure 4 : Luminescence intensity dependence
on intensity of incident light for He-Ne laser
excitation. Area of illumination a) $\sim 10^{-2}$ mm²
b) $\sim 5 \times 10^{-2}$ mm² c) ~ 1 mm²

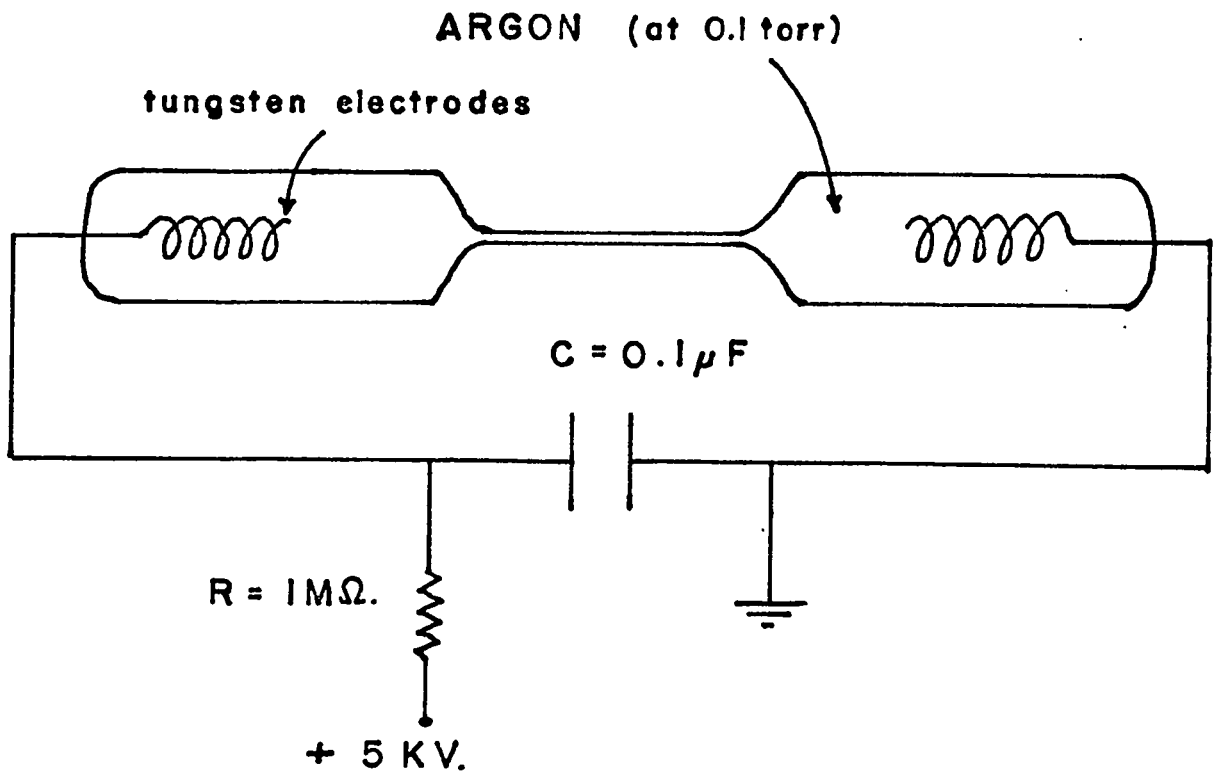


essential difference between the two processes is that in (1), the concentration of excited states is increased for the same number of luminescent centers, and in (2), the number of centers is decreased while the concentration of excited states is increased.

Measurements of the luminescence response time (combined rise and decay times) were made using high intensity argon flash tubes built in the laboratory. A diagram of a typical tube is given in Fig.5 together with the values of the discharge capacitances and voltages used. The Pyrex tubes were sealed at a pressure of 0.1 torr and had a rise time of 0.5 μ sec. with a characteristic peak intensity of width 0.1 μ sec.. The light intensity output in the visible region was approximately constant with wavelength and the light was directed on to the sample after wavelength selection by a grating monochromator. The luminescence was found to follow the pulse form exactly at 300 and 77°K for all excitation wavelengths. This implies that the response time for the luminescence is $\leq 10^{-7}$ sec. which is in agreement with previous work by Karkhanin and Vorob'ev (1962), for a luminescence at about 0.8 μ .

The speed of response of the luminescence suggests that the non-linearity discussed above is more probably due to a saturation of the lower level

Figure 5 : Argon flash tube design.



in the luminescent decay process rather than to pair annihilation of the excited state as suggested by Tolstoi and Abramov (1967).

Further experimentation with the He-Ne laser and monochromatic light from the monochromator showed that the excitation spectrum did not change measurably when polarised light was used. Neither was the emission polarised nor was its direction of propagation dependent on the direction or polarisation of the incident light beam. The luminescence therefore, although of fast response, has no "memory" of the nature of the excitation process, as far as these properties are concerned.

Conclusion to Chapter 2 : In this chapter, we have laid the basis for more detailed experimentation. Most of the measurements described are necessary to give an overall picture of the luminescence mechanisms and to thus permit the choice of a suitable model.

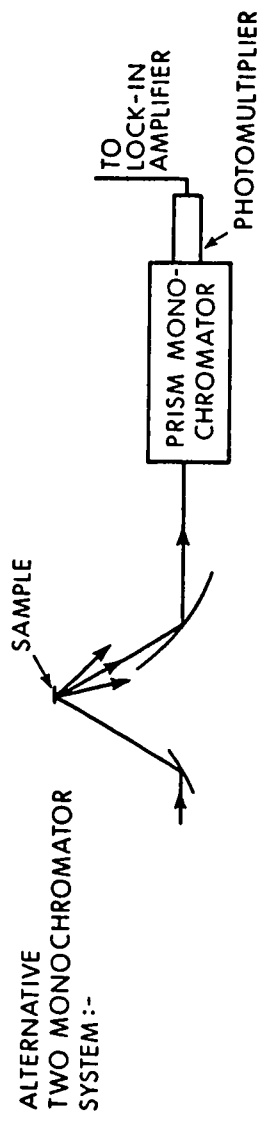
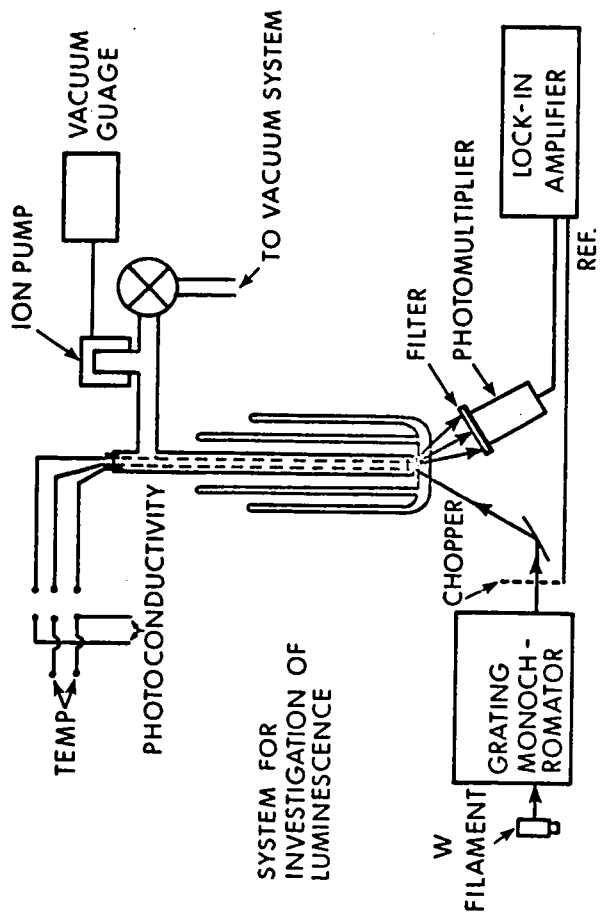
CHAPTER 3.

Excitation Spectra for Luminescence.

For the experiments described in this chapter the sample handling techniques were similar to those used in earlier work in this laboratory (Fortin (1965)) and they have subsequently been described in detail by Zielinger et al. (1968). In brief, the sample to be studied was provided with sputtered platinum contacts wrapped with platinum foil and was then suspended in a clear quartz tube by a set of two chromel-alumel thermocouples. A small electrical oven or Pyrex double dewar with a flat bottom could alternatively be mounted around the quartz tube giving a temperature range from 1000°C down to 4.2°K. For improved heat exchange at low temperatures a heated quartz capillary was used as a controlled helium leak.

The investigations of the luminescence excitation spectra discussed in this chapter were carried out using the system shown schematically in Fig.6. This consisted of a motor driven Bausch and Lomb model 33-86-45-59 monochromator with wolfram ribbon lamp as light source. The monochromator output was focussed by means of a concave front surfaced

Figure 6 : Cryostat and experimental arrangement for measuring luminescence and photoconductivity.



aluminum mirror into the double dewar and on to the sample in the quartz tube. The incident light was chopped at 80 Hz and the luminescence detected by means of a photomultiplier with S1 response (RCA number 5102). The luminescent signal was amplified by a lock-in amplifier and recorded on a chart recorder.

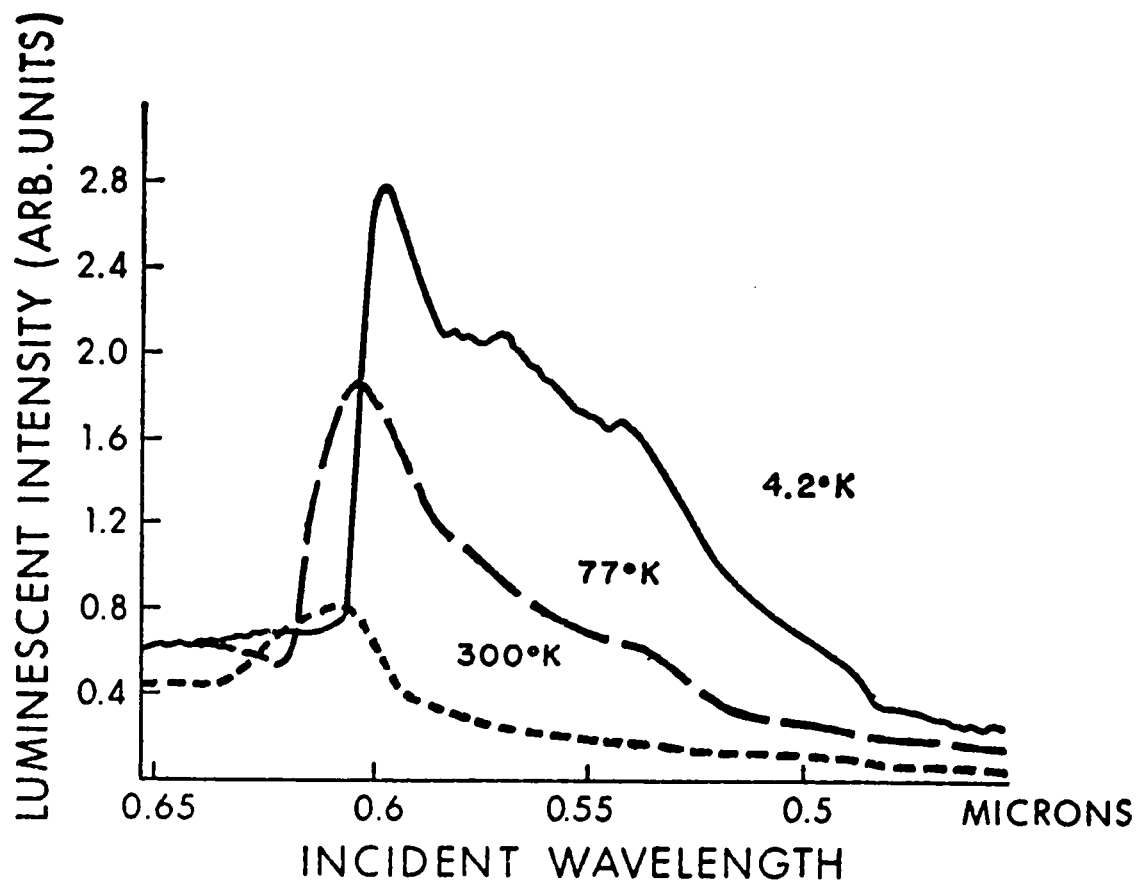
To restrict the radiation incident on the photomultiplier to the luminescence, all visible light was excluded by an interference filter peaked at 0.96μ .

The sample and detector were completely surrounded by a light-tight enclosure.

In the analysis of the emitted radiation discussed in chapter 1, a Leiss quartz prism double monochromator was used, making up the two-monochromator system shown in Fig.6 as an alternative configuration.

The excitation curves for luminescent intensity versus incident wavelength for a sample having strong luminescent response are shown in Fig.7, for temperatures of 300, 77 and 4.2°K . The position of the peak and long wavelength edge are seen to shift to longer wavelengths while the overall intensity increases as the temperature is reduced. The temperature dependence of the luminescence has been described in the previous chapter. The shift of the peak and long wavelength edge is in strong correlation with

Figure 7 : Luminescence excitation curves for a strongly emitting sample whose room temperature quantum efficiency was 5%. The three curves shown are for temperatures of 300, 77 and 4.2°K.

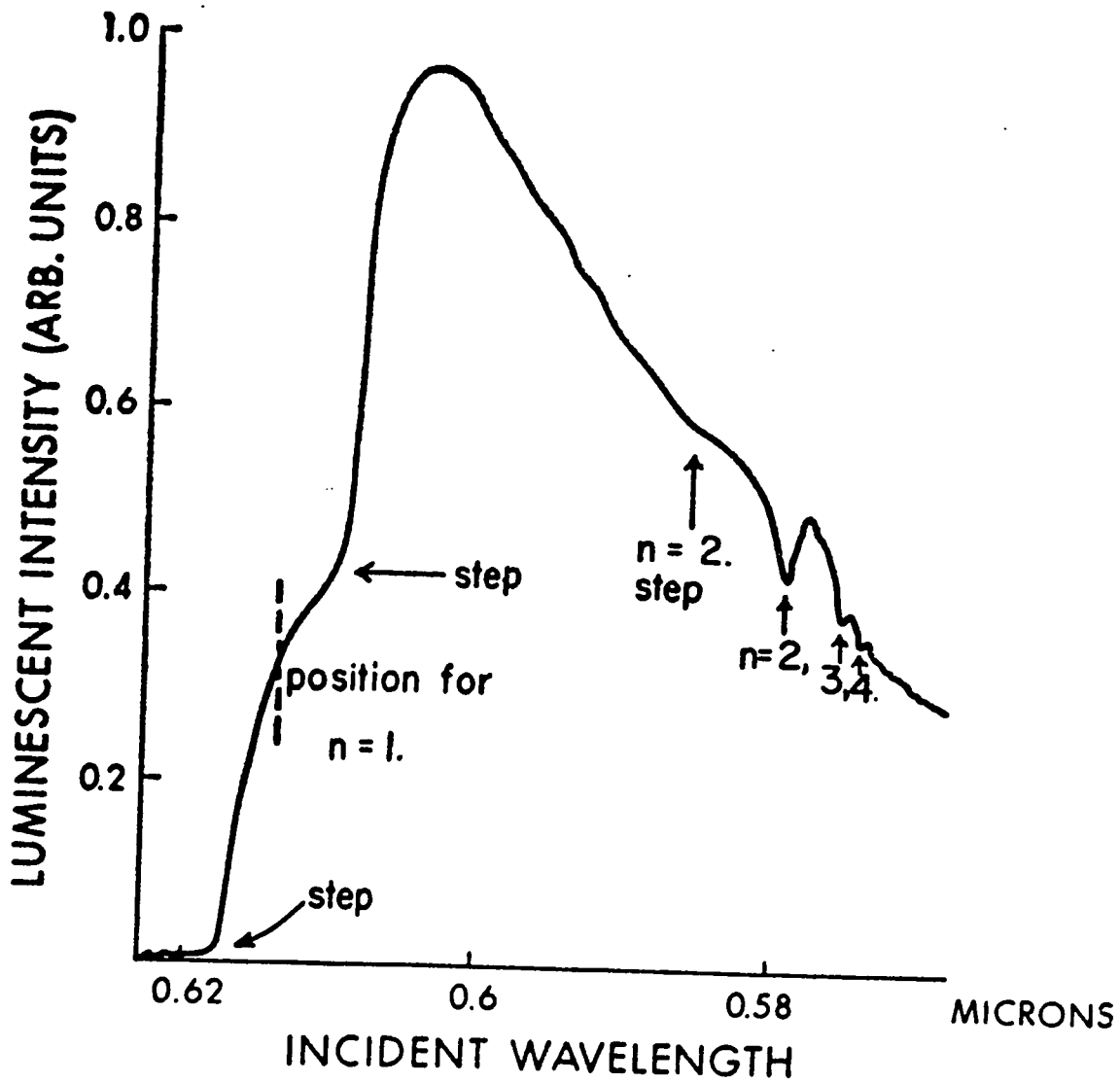


the known temperature shift of the absorption edge of the material. This effect which is due to the shift in band structure as the temperature is decreased has been discussed by Weichman (1960) and we see that the position of the luminescence long wavelength edge corresponds exactly to the known position of the absorption edge for the three temperatures shown, 300, 77 and 4.2°K.

The luminescence is thus seen to be associated with the intrinsic absorption processes in the material. This result is more strikingly demonstrated for a weakly emitting sample. We define weakly emitting samples to have a maximum room temperature quantum efficiency η of less than 0.1%. Similarly, strongly emitting samples are those whose quantum efficiency under equivalent conditions is greater than 1%.

The choice of these two sample categories was based on the overall curve shapes they displayed. Thus Fig.7 shows curves which are characteristic of a strongly emitting sample where there is still appreciable luminescence for the exciting wavelength region $\lambda < 0.56\mu$ at 77 or 4.2°K. A weakly emitting sample on the other hand shows a considerably simpler overall curve shape, as in Fig.8. Here a single peak at 0.6 μ is observed with a sharp cut-off on the

Figure 8 : Luminescence excitation curve for a weakly emitting sample of quantum efficiency $\sim 0.1\%$ at 300°K . Exciton structure can be easily resolved. The temperature of measurement was 77°K .



wavelength edge at 0.62μ for a temperature of 77°K . The short wavelength edge decreases monotonically to zero at about 0.55μ with the exception of some fine structure in the range 0.58 to 0.57μ , which we attribute to excitons.

These overall curve shapes for the two types of samples have been found to hold for a number of samples and no exception to the rule has yet been observed. The intermediate quantum efficiency range $\eta = 0.1$ to 1% shows curves intermediate between the two types described.

The most interesting property of the weakly emitting samples is that exciton structure can be readily resolved. (This is not the case for strong emitters, possibly due to the complexity of the excitation curves, although some structure can be seen for thin samples.) Fig.8 clearly shows a pronounced dip at exactly the wavelength of the $n=2$ exciton absorption line of the yellow series at 77°K . Further, dips corresponding to $n=3$ and 4 can also be observed. This type of exciton structure had not been previously reported for luminescence although exciton effects in photoconductivity excitation curves are well known.

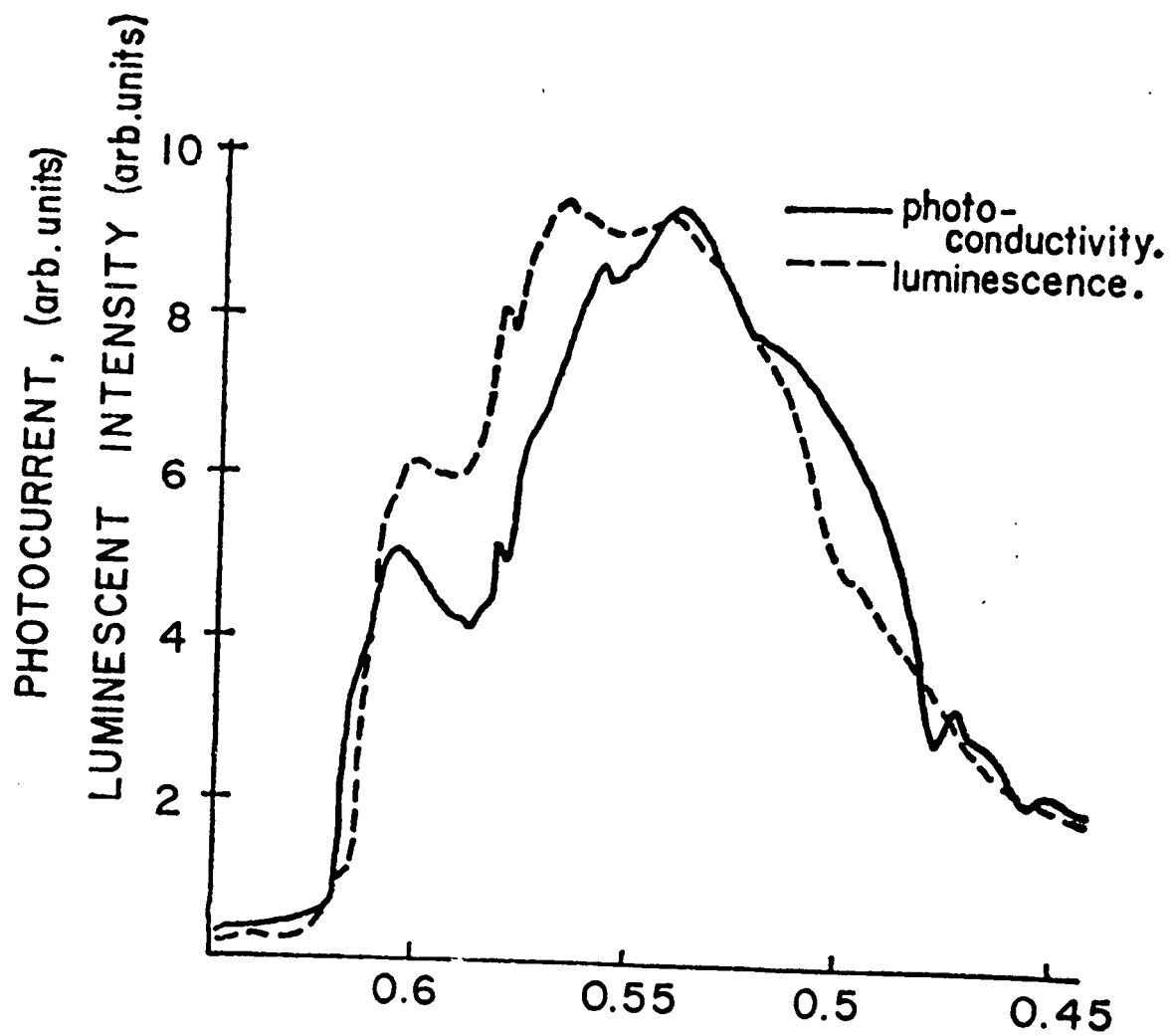
A photoconductivity curve for a strongly

emitting sample is shown in Fig.9 with a luminescence excitation curve for a thin crystal prepared from the same sample for comparison. The thin crystal enables us to resolve some weak exciton structure as mentioned above and we may see from Fig.9 that there is a similarity between the excitation curves for the two effects. It was found during later experiments, however, that correlations between luminescence and photoconduction are highly unreliable.

Conclusion to Chapter 3 : In the experiments described here, the luminescence excitation curves for a number of samples of different quantum efficiency were measured.

It was found that two types of curves could be distinguished corresponding to strong and weakly emitting samples whose room-temperature quantum efficiencies were $>1\%$ and $<0.1\%$ respectively. The position of the cut-off edge on the long wavelength side, together with the observation of exciton structure, suggests that the luminescence is closely related to the intrinsic absorption processes of the material which take place at identical wavelength regions.

Figure 9 : Photoconductivity excitation curve for a strongly emitting sample, shown together with a luminescence excitation curve for a thin crystal prepared from a similar sample. The temperature of measurement was 77°K.



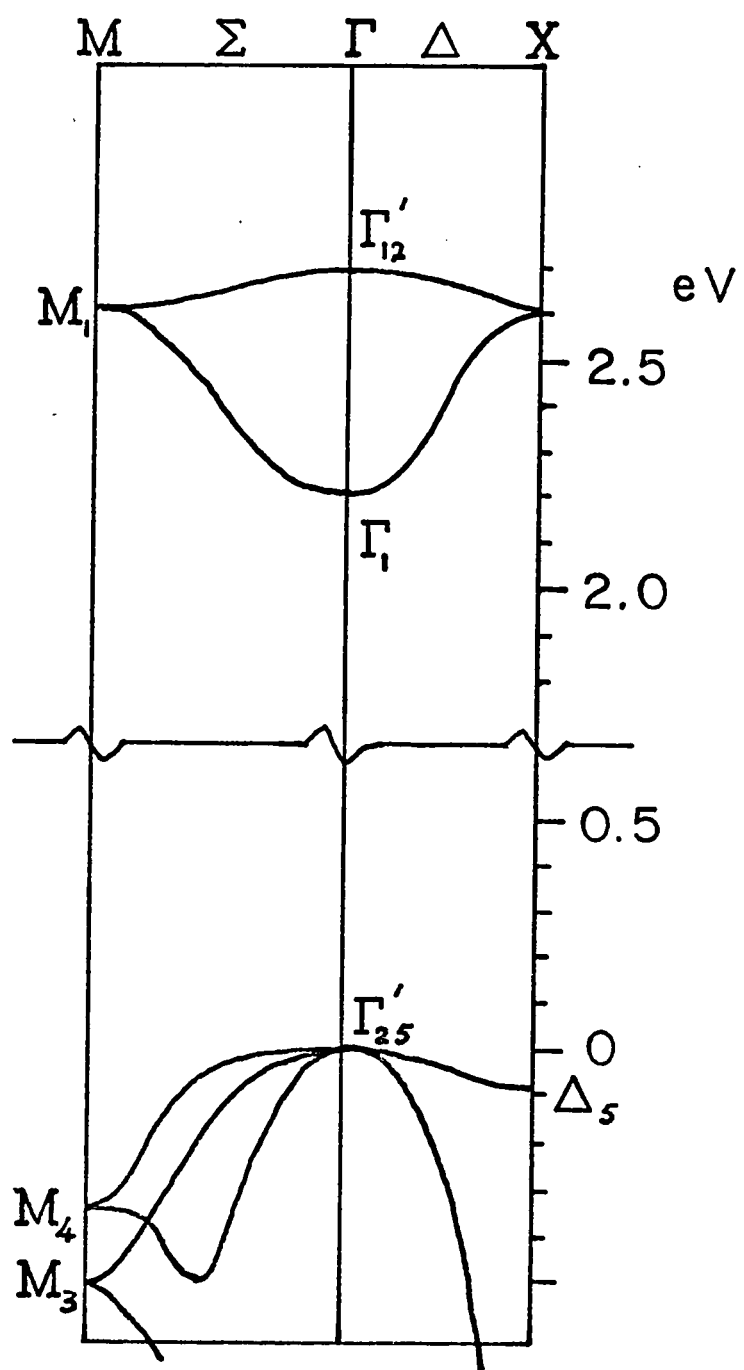
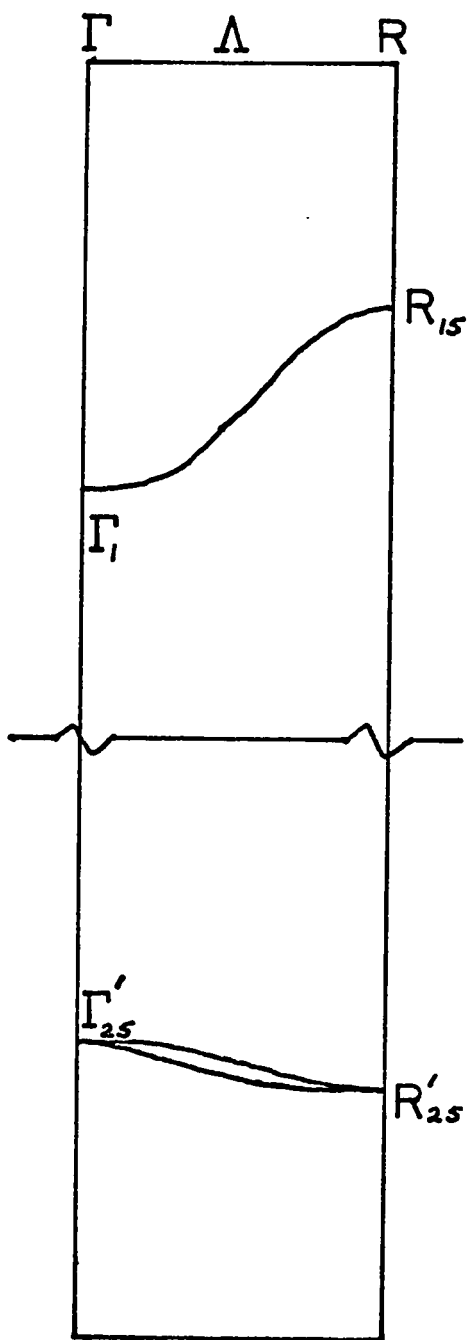
CHAPTER 4.

Band Structure and Absorption Processes.

Calculations on the band structure of Cu_2O have been made by Elliott (1961) and Zhilich and Makarov (1961), while a more detailed band scheme extending the findings of these authors to cover the whole of the Brillouin zone was later computed by Dahl and Switendick (1966). Their scheme is reproduced in Fig.10 for the bands of interest to us here, ie. the valence and conduction bands. We have also corrected their scheme to fit the experimental band-gap results at 77°K and it is thus hoped that the scheme is now a good description of the electronic states of the material. (See Dahl et al. (1966))

We first note that both the valence band and the first conduction band are highly "spherical" about the band minima at $\underline{k} = 0$. This result, which at one time was assumed to be true for most semiconducting materials, is now found to be very rare. Also, the curvatures of the valence and first conduction bands are seen to be similar, giving approximately the same effective mass for electrons and holes. The "sphericity" of the bands means in this case that these effective

Figure 10 : The band structure of Cu_2O in the region of the valence and conduction bands. Temperature is 77°K . (After Dahl and Switendick (1966)).



masses are isotropic in the material.

If we again return to Fig.10, we find that the $\tilde{k} = 0$ symmetries of the valence and first conduction bands are Γ'_{25} and Γ_1 respectively, and since the Γ'_{25} and Γ_1 symmetries both have even parity, (under reversal of spatial co-ordinates) electric dipole transitions between Γ'_{25} and Γ_1 are forbidden.

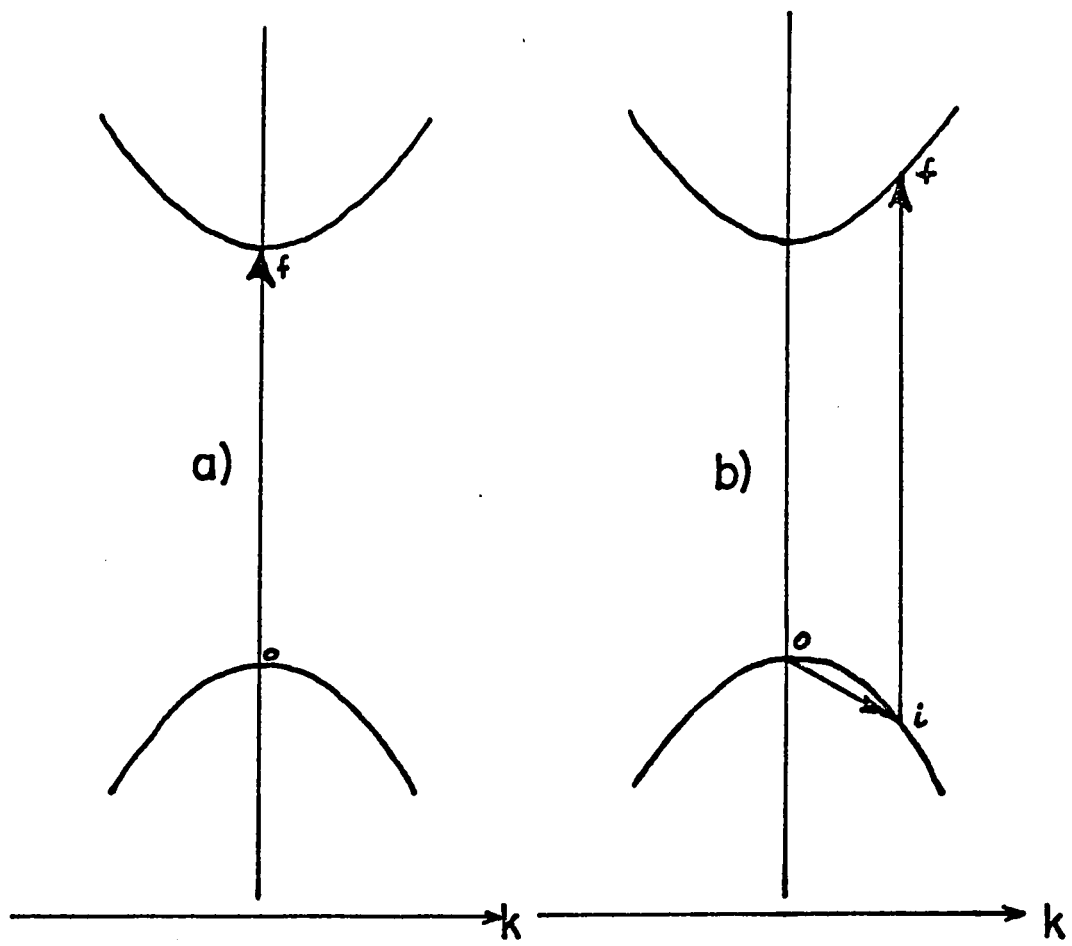
These are the "direct" transitions involving a photon energy $h\nu_g$ which would transfer an electron in the valence band at Γ'_{25} to the conduction band at Γ_1 ($h\nu_g$ here is the band-gap energy). For this type of transition, the momentum of the incoming photon can be considered to be negligible (compared to the momenta of the electrons and holes), and the overall momentum conservation becomes

$$\tilde{k}_e + \tilde{k}_h = 0 \quad 3)$$

and the electron and hole created have equal and opposite momentum. These transitions appear as vertical on the band scheme in Fig.11.

However, since transitions $\Gamma'_{25} \rightarrow \Gamma_1$ are forbidden, the first allowed transitions are from the valence band Γ_1 to the upper conduction band Γ'_{12} at 2.7 eV.

Figure 11 : Direct and Indirect transitions
as they appear on the band scheme. Process a) Direct,
b) Indirect.



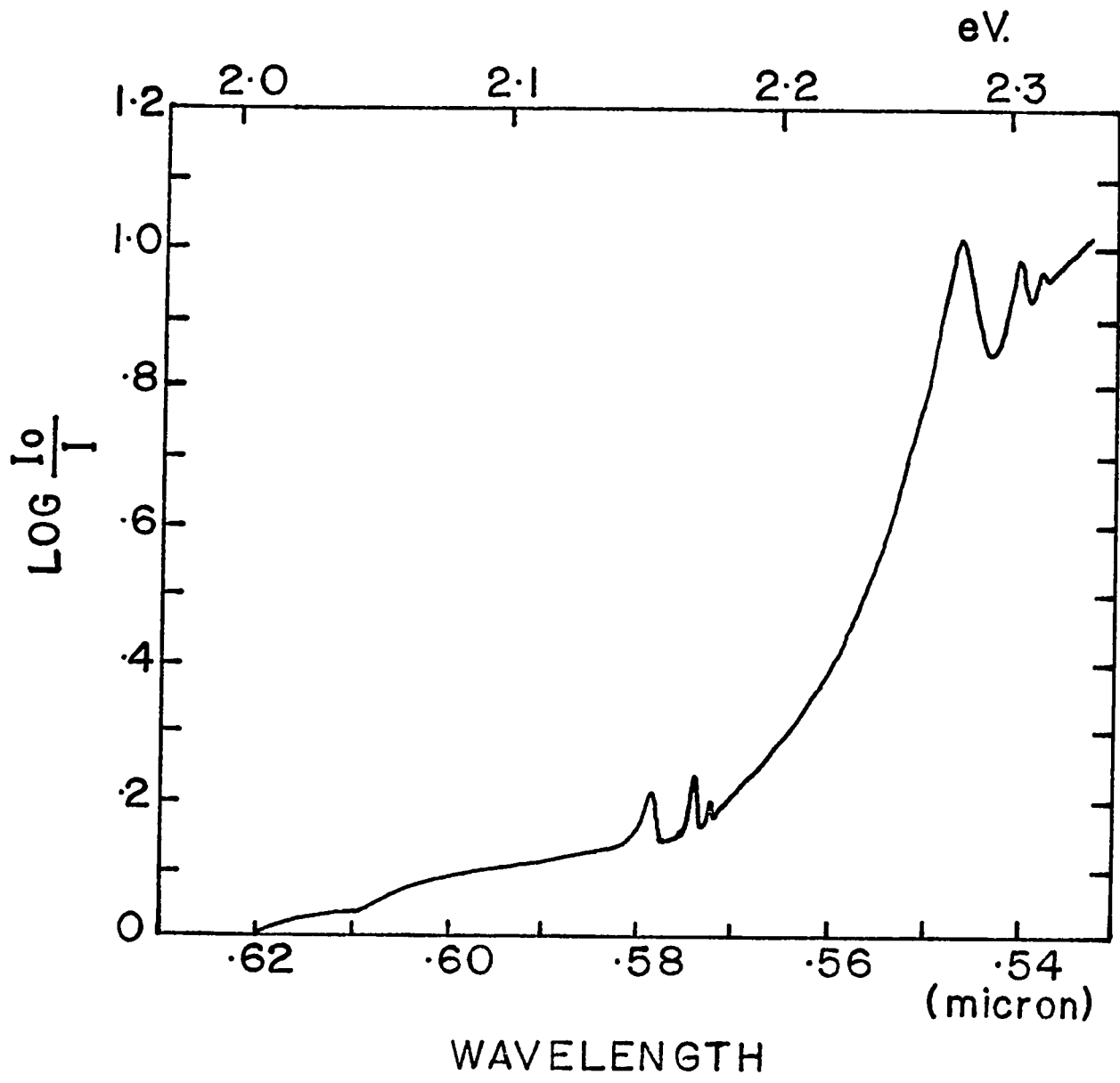
The experimental absorption results in Fig.12 show an absorption edge at about 2.0 eV at 77°K together with two series of hydrogenic type absorption lines fitting a Rydberg series for $n=2,3,4,5 \dots$ etc. (Nikitine (1955), Nikitine (1959), Baumeister (1961)).

The theory has been further developed to include these results by concluding that since direct transitions $\Gamma'_{25} \rightarrow \Gamma_1$ are forbidden, indirect transitions involving the absorption or emission of a lattice phonon become important. Further, the two hydrogenic absorption series have been attributed to the creation of exciton states (electron - hole bound pairs) in the material. Since the electrons and holes of the excitons are associated with the Γ_1 and Γ'_{25} conduction and valence bands respectively, direct transitions to these exciton states are also forbidden. The oscillator strength for direct transitions to the exciton states has been calculated by Elliott (1957) who gives the following expression

$$f = C \frac{n^2 - 1}{n^5} \quad 4)$$

where n is the principle quantum number (analogous to the hydrogen model) and C may be considered to be constant for a particular exciton series.

Figure 12 : Absorption curve for Cu_2O at 77°K . (After Grun (1962))



We see that for direct transitions to $n=1$, the oscillator strength is zero and these transitions are strictly forbidden. For $n=2,3 \dots$ etc. however, there does remain a small oscillator strength giving rise to absorption at the energy of these excitons due to direct transitions which take place essentially at $\underline{k} = 0$.

This explains therefore the experimental absorption results of Fig.12 where the two hydrogenic series of absorption lines are seen for $n=2$ and higher, but no absorption lines are observed for $n=1$. (Note : To be strictly accurate here, there does remain a small absorption line for $n=1$ of the yellow series at 0.61μ for a temperature of 77°K . This line however is due not to electric dipole, but to electric quadrupole transitions, which expression 4) does not include) (Elliott (1961), Grun and Nikitine (1962)).

The presence of two exciton series, "yellow" and "green", has been attributed to a spin-orbit splitting of the Γ'_{25} valence band with a splitting energy of 0.13 eV . The yellow series thus arises due to the formation of excitons by conduction electrons Γ_1 and the holes in the upper valence band. Similarly, the green series is associated with electrons in the conduction band Γ_1 and holes in the lower valence band.

As yet, however, we have given no explanation for the absorption edge which occurs at even lower energy than the $n=2$ of the yellow series and which constitutes a strong continuous background up to and beyond this exciton line. This problem was resolved on observing the presence of two distinct steps on the absorption edge at 0.62 and 0.61μ (see Fig.12). Elliott (1960) interpreted these steps to be due to indirect transitions to the $n=1$ exciton of the yellow series with the absorption or emission of a single phonon. The frequency of the phonon is simply derived from the energy separation of the two steps and is found to be 105 cm^{-1} . Also the position of the $n=1$ exciton state is found to be 0.6126μ , since it is simply midway between the two steps.

We see therefore that all absorption in the range $0.62 \rightarrow 0.56\mu$ is due to indirect transitions to the $n=1$ exciton of the yellow series with the exception of the small superimposed lines for direct transitions to the $n=2,3,4$ etc. No evidence was found in absorption work of the $n=1$ level of the green series.

We have said that the higher energy electric dipole transitions $\Gamma'_{25} \rightarrow \Gamma'_{12}$ to the second conduction band are allowed and, in fact, two lines have been observed in both absorption and photoconduction work

(Dahl et al. (1966)) at 2.6 and 2.7 eV which have been attributed to direct transitions to the n=1 exciton levels of a "blue" and "violet" series respectively.

Conclusion to Chapter 4 : We have reviewed the optical absorption results and the theory which has been developed to account for them. It is seen that direct transitions $\Gamma'_{25} \rightarrow \Gamma_1$ are forbidden. Direct transitions to the exciton states associated with these bands are also forbidden and it is expected that indirect processes with the absorption or emission of a phonon become important. The optical absorption in the range $0.62 \rightarrow 0.56\mu$ at 77°K is thus believed to consist of a broad background absorption due to indirect transitions to the n=1 exciton of the yellow series with a series of sharp lines superimposed which are due to direct transitions to the n=2,3 ...etc. exciton levels.

CHAPTER 5.

Luminescence Excitation Processes and the Exciton Line Shape Problem.

In the preceding section it was shown that the absorption in the region of interest for luminescence was predominantly to the $n=1$ exciton of the yellow series with the exception of the weak absorption lines for direct transitions to $n=2$ and higher exciton levels. We thus expected that the luminescence, which is excited in the visible range, would be associated in some way with exciton levels since these are the intrinsic excited states of the material in the range indicated. The possibility remained however, that the luminescence was entirely associated with the extrinsic luminescent center, ie. that the absorption giving rise to luminescence bore no relation to the absorption producing the excited states of the bulk material.

The problem was resolved however during the studies on weakly emitting samples. For these samples, exciton structure is readily resolved as was shown previously in Fig.8. If we again consider Fig.8, and the significant structure which is indicated

in this excitation curve, the relationship between luminescence and the excitation processes of the bulk material becomes clear. Two steps are seen on the long wavelength edge of the excitation curve which correspond exactly to these occurring in the absorption coefficient. Further, the $n=2,3$ and 4 exciton lines for absorption also appear in the luminescence as dips in the curves. It is clear therefore that the luminescence is closely associated with the intrinsic absorption of the material and we have seen in the previous section that this is predominantly to the $n=1$ exciton level of the yellow series. That the $n=2,3$ and 4 exciton lines appear as dips in the excitation curves suggests that these excitons are not as likely to produce luminescence as $n=1$.

One of the most striking results of this excitation curve analysis was the resolution of the well known exciton line asymmetry problem (Taylor and Weichman (1969)). It has long been known from absorption measurements that the higher exciton absorption lines (the $n=2$ of the yellow series in particular) were highly asymmetrical in shape. The $n=2$ line shows a long "tail" on the long wavelength (low energy) side with a sharp cut-off on the high energy side. This result had been interpreted by Elliott (1960) to be due to a

mixture of indirect processes to $n=1$ and direct processes to $n=2$ in the region of the $n=2$ absorption line. He finds the following expression for the absorption coefficient due to indirect processes only

$$\alpha = \frac{4\pi^2 e^2}{\eta mc^2 v} \left| \frac{\sum_i \langle 0 | \underline{\epsilon} \cdot \underline{p} | i, 0 \rangle \langle i, 0 | H_{e1} | 1s, \underline{K}; n_{\underline{K}} \pm 1 \rangle}{E(i, 0) - E(1s, \underline{K}) \pm E_p(\underline{K})} \right|^2 \times \rho(1s, \underline{K}) \quad 5)$$

where ϵ is a vector parallel to the electric vector of the incident light, p is a momentum matrix element, H_{e1} is the electron lattice interaction transferring the electron from the intermediate state $|i, 0\rangle$ to the final state $|1s, \underline{K}\rangle$, ρ is the density of states and E_p is the phonon energy (see Appendix A).

The set of intermediate states $|i, 0\rangle$ likely to be important are at Γ'_{12} since here elements $\langle 0 | \underline{\epsilon} \cdot \underline{p} | i, 0 \rangle$ are non-zero and transitions $|0\rangle \rightarrow |i, 0\rangle$ are not forbidden. However, as we have already seen, there does remain a small oscillator strength for electric dipole transitions to the $n=2$ and higher exciton levels, and so there is a small contribution in expression 5) due to indirect transitions to $n=1$ via $n=2$ as intermediate state since elements $\langle 0 | \underline{\epsilon} \cdot \underline{p} | 2p, 0 \rangle$ are small but non-zero.

Elliott thus finds that the absorption line

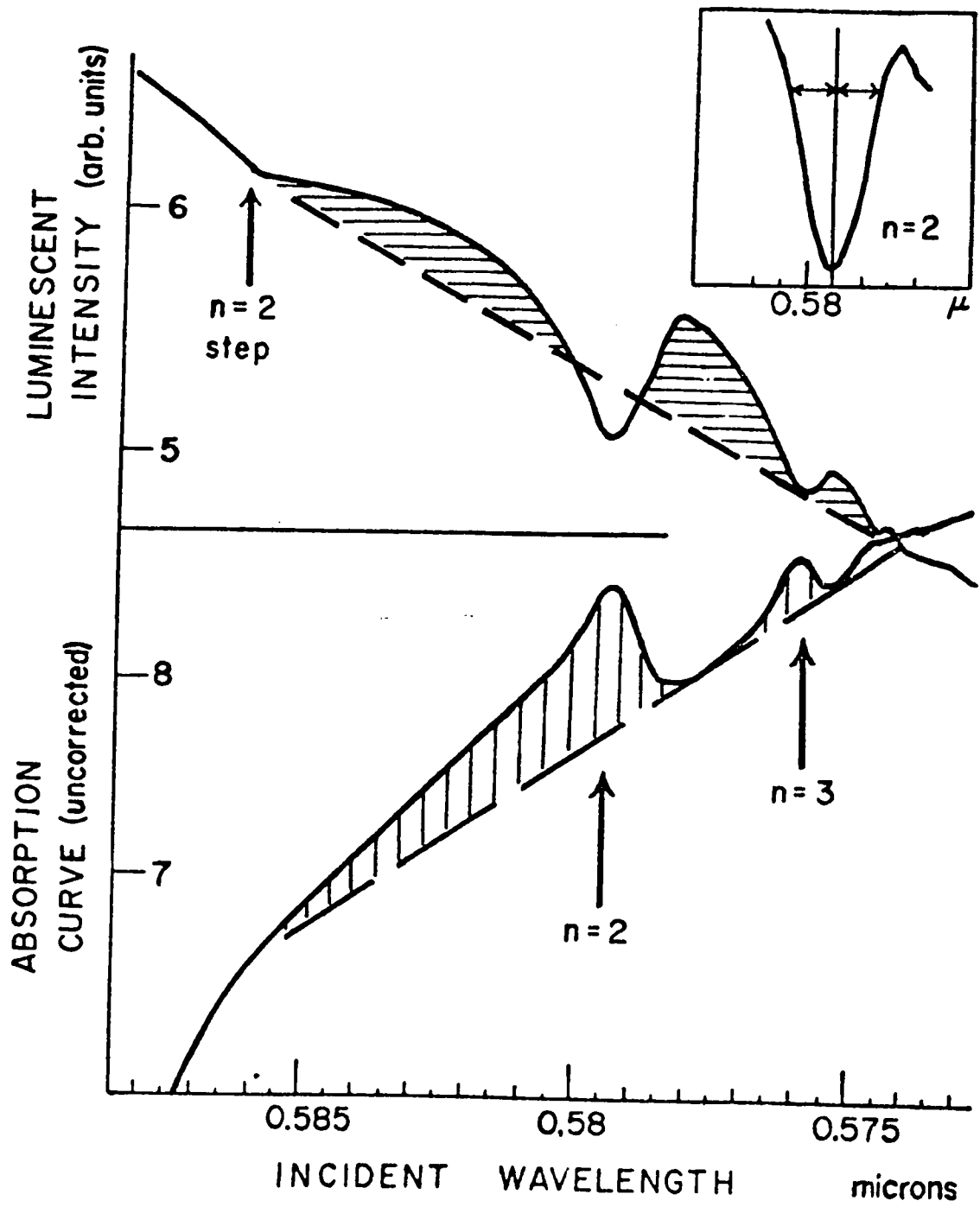
asymmetry is due to an increasing absorption to $n=1$ due to phonon assisted transitions via $n=2$ as the wavelength of the $n=2$ line is approached. At exactly the wavelength of the $n=2$ line, however, direct transitions to the $|2p,0\rangle$ exciton states are possible due to the small oscillator strength for these processes as discussed above, and $n=2$ excitons are created.

We were able to resolve this problem and show that Elliott's theory was valid by careful measurement of our luminescence excitation curves in the region of the $n=2$ line.

A step and initial increase was observed in the excitation curve as the $n=2$ line was approached. At the wavelength of the $n=2$ line, however, the luminescence decreased sharply below background and a dip was produced in the curve. Similar structure was seen for $n=3$. A detail of this part of the excitation curve for the sample shown in Fig.8 is given in Fig.13 together with an uncorrected absorption curve for the same sample in the same wavelength region for comparison. The absorption curve shows the familiar asymmetrical line whereas the luminescence structure shows the step and increase in luminescence (shaded area) followed by the sharp dip. On higher amplification, (inset Fig.13) this dip was seen to be

Figure 13 : A detail of the luminescence excitation curve of Fig.8 in the region of $n=2$ of the yellow series. An uncorrected absorption curve for the same sample in the same region is also shown for comparison. Temperature is 77°K .

Inset : detail of the $n=2$ dip in luminescence, showing a high degree of symmetry.



highly symmetrical.

We interpret these findings to be due to the result that the luminescence takes place predominantly from the $n=1$ exciton states of the yellow series. Thus the initial increase above background is due to increased absorption to $|1s, \underline{k}\rangle$ via the $|2p, 0\rangle$ levels as intermediate states. However, as the wavelength for direct transitions to the $|2p, 0\rangle$ states is approached, the optical absorption populates this exciton level, which therefore produces a competing process for transitions to $|1s, \underline{k}\rangle$ and a decrease in luminescence is observed. The symmetry of the dip in the excitation curve reflects the symmetry of the direct absorption processes to $n=2$ (for matrix elements $\langle 0 | \underline{g} \cdot \underline{p} | 2p, 0 \rangle$).

The steps and dips discussed here are strongly reminiscent of those observed in photoconductivity for the "blue" and "violet" absorption lines (see for example the photoconductivity curve of Fig.9, where the dips in question appear at 0.48 and 0.46μ respectively).

As was indicated in the preceding chapter, these two dips and the corresponding lines in absorption have been attributed to excitons associated with the direct transitions $\Gamma'_{25} \rightarrow \Gamma'_{12}$ at $\underline{k} = 0$ (Dahl et al (1966)).

The energy separation of the two lines agrees well with the spin-orbit splitting energy of the valence band of 0.13 eV. However, we would not expect steps to appear in photoconductivity excitation curves for allowed transitions. We have therefore tentatively suggested that the steps and dips correspond to indirect transitions to the same band as given by Γ'_{12} but to the edge of the zone instead of at $\underline{k} = 0$, since the density of states is more favourable here than at $\underline{k} = 0$ owing to the curvature of the bands (see Fig.10). The important intermediate states for the process would be at Γ'_{12} .

Conclusion to Chapter 5 : We have shown here that these luminescence measurements are a valuable means of studying the absorption processes in the material since the excited states for the 1μ luminescence are those of the bulk material. Further, the luminescence appears to be predominantly associated with the $|1s, \underline{k}\rangle$ exciton levels and it is this effect which allows the direct and indirect processes in the region of the $n=2$ exciton absorption line to be resolved.

CHAPTER 6.

Thickness's Dependence and Exciton Structure.

It was seen in an earlier chapter that the overall shape of the luminescence excitation curves depended on the thickness of the sample. This result was seen for both strong and weak emitters (compare for example Figs. 7 and 9), although as usual the weak emitters showed the most pronounced exciton structure.

It was therefore decided that a careful study should be made of this effect, and since the experimental evidence up to this point showed that the luminescence was a bulk property and was not influenced by exposure of the sample to air (as is photoconductivity), a new cryostat with an improved optical arrangement was designed.

The equipment used for light sources and wavelength selection was the same as used in the earlier system (Fig.6), but the detection system was re-arranged whereby the S1 photomultiplier with Corning 2540 filter was incorporated into the cryostat and the whole system including the potential divider and anode load resistor system for the photomultiplier cooled directly in liquid nitrogen.

A light-tight box was fitted around the cryostat to reduce the background signal and the samples were mounted on a thick glass substrate for ease of handling and polishing. The incident light was again chopped and the photomultiplier signal detected using a lock-in amplifier. The frequency used was 80 Hz. A schematic of this cryostat is shown in Fig.14. Over a number of runs neither the photomultiplier nor the filter showed any signs of deterioration and other than some changes in the transmission spectrum of the filter in going to low temperatures, no difficulties with the system were encountered. Further, the new system achieved increased sensitivity and a lower noise level.

With this system it was possible to make detailed studies on weakly emitting samples with good spectral resolution. Structure corresponding to the weak $n=1$ electric quadrupole line was observed together with dips at the wavelengths of $n=2,3,4$ of the yellow series and $n=2,3$ of the green series (Fig.15a). This completes for luminescence the sets of exciton structure known from previous absorption and photoconduction work.

On reducing the thickness of the samples however, a new size effect in Cu_2O was observed in which

Figure 14 ; Schematic of the liquid N₂ cryostat used for detection of luminescence from weakly emitting samples.

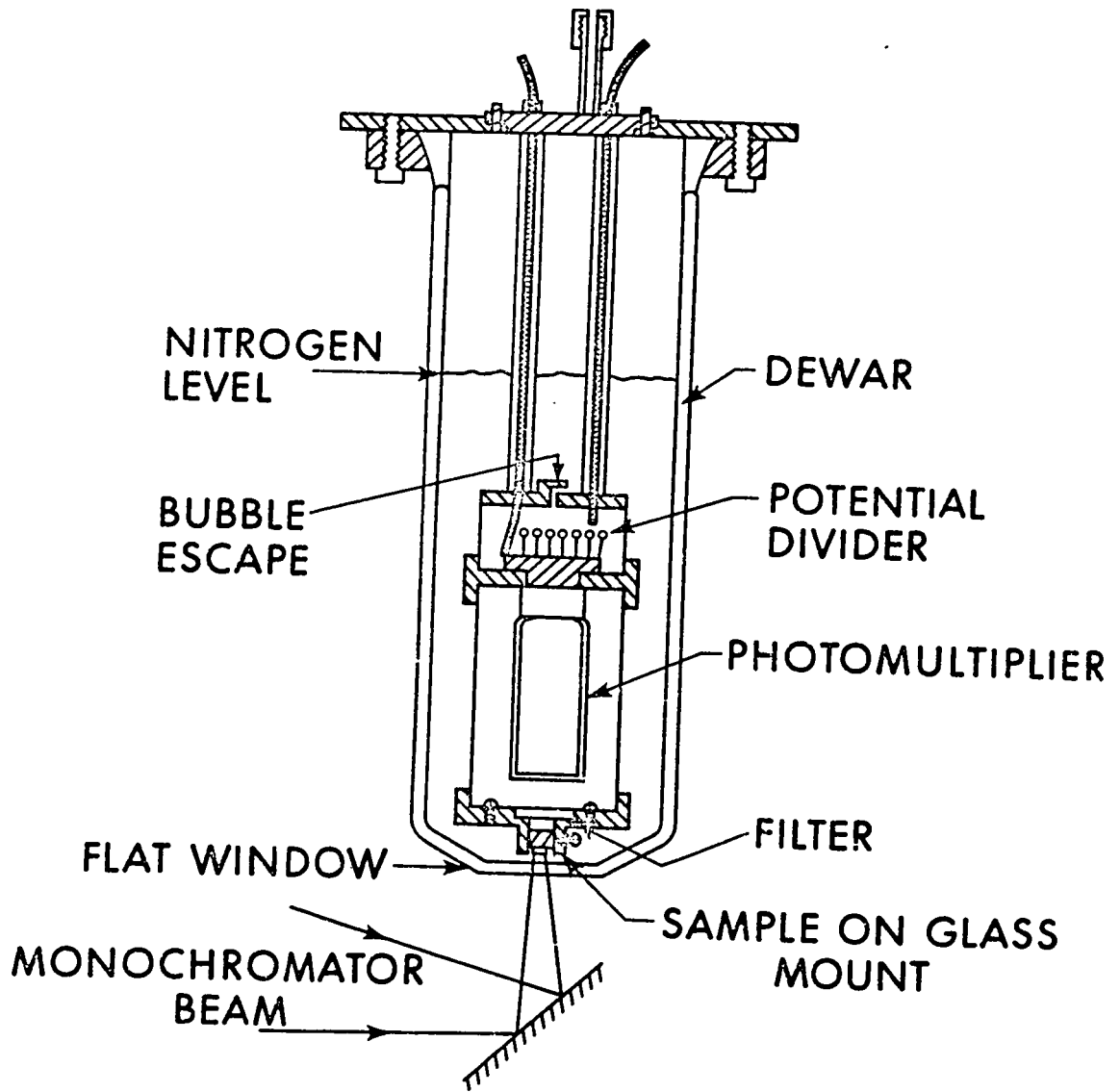
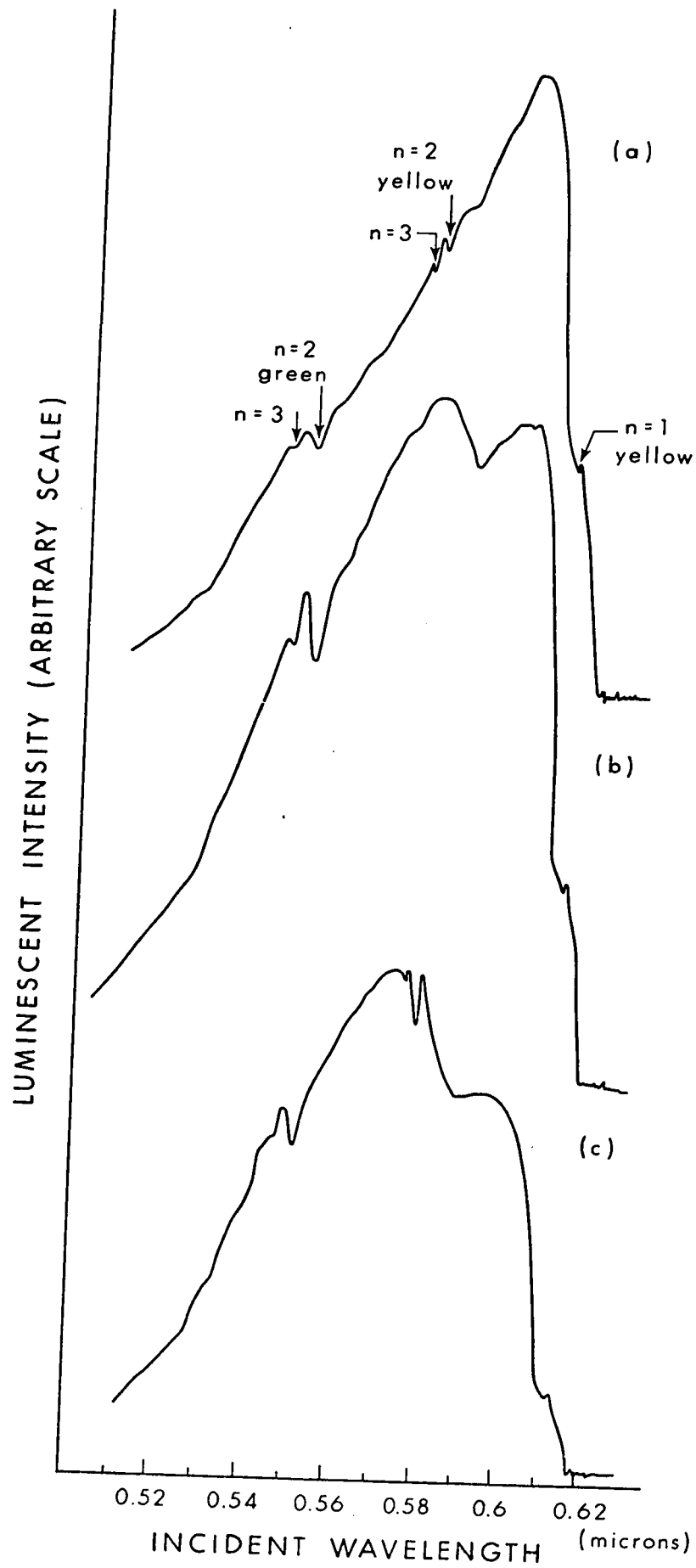


Figure 15 : Luminescence excitation curves for a weakly emitting sample for the three thicknesses a) 0.1 cm b) 0.0045 cm c) 0.003 cm at a temperature of 77°K. The inversion of the n=2 dip of the yellow series as the thickness is reduced is clearly seen, and further, the overall shape of the excitation curve is changed with the maximum moving to shorter wavelength.

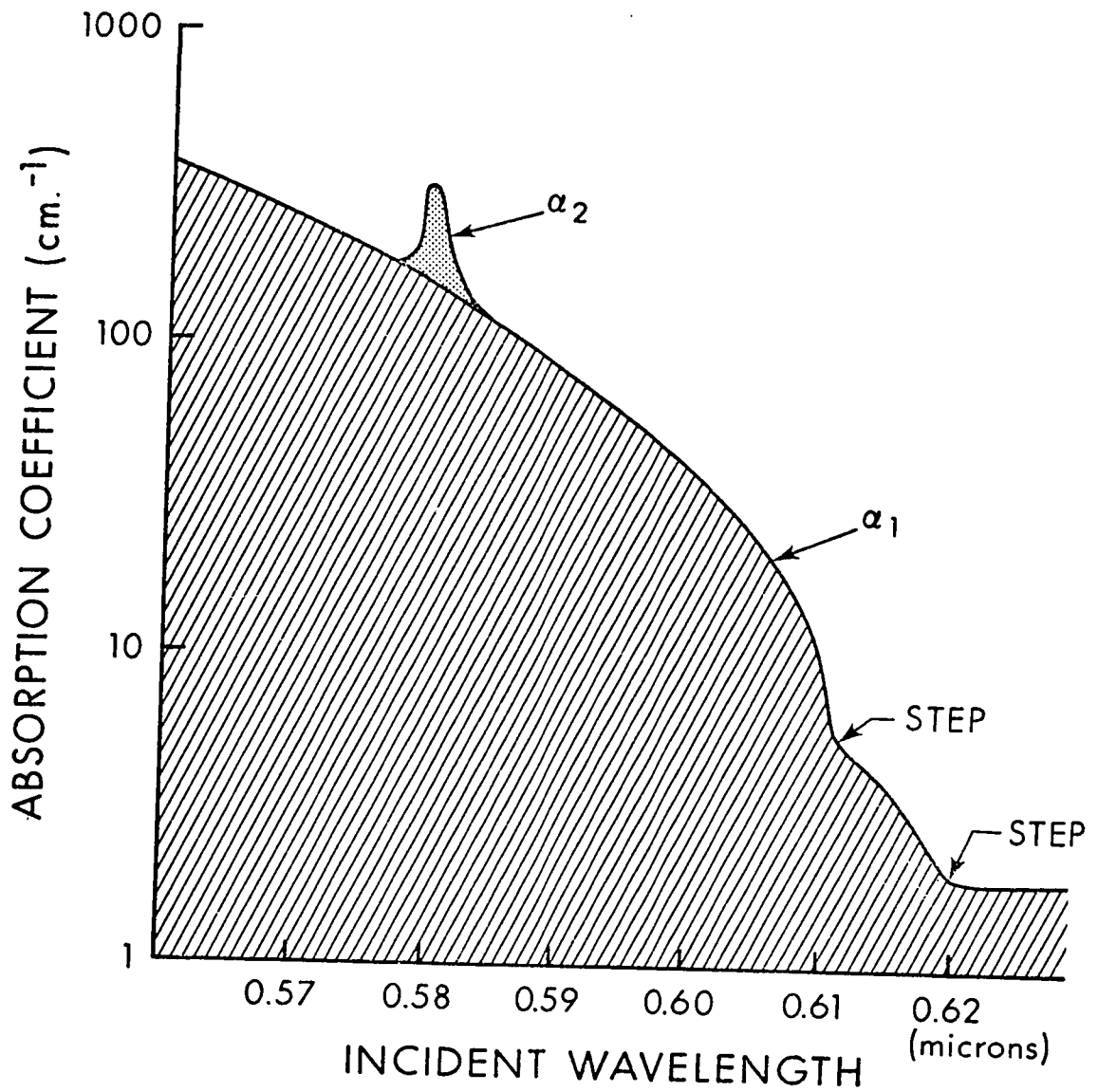


the $n=2$ dip for the yellow series could be made to invert to a peak for thin samples. At the same time, the overall shape of the excitation curves changed significantly with decreasing sample thickness, with the peak position shifting to shorter wavelengths.

Figures 15a, 15b, and 15c show the influence of the size effect. In Fig.15a, sample thickness 1 mm, the $n=2$ lines of both the yellow and green series appeared as dips. On successively reducing the sample thickness by grinding and polishing, the $n=2$ dip of the yellow series could be made to disappear (Fig.15b) and on reducing the thickness still further, peaks corresponding to the $n=2,3$ of the yellow series could be observed (Fig.15c), while the $n=2$ line of the green series remained as a dip.

Bearing in mind that this wavelength region from 0.56 to 0.62μ corresponds to a range of rapidly varying absorption coefficient (see Fig.12), we can set up a model for luminescence since we know the nature of the absorption processes as discussed earlier in Chapter 4. We show in Fig.16 a simplified curve of the absorption constant α as a function of wavelength in the range 0.56 to 0.63μ , ie. in the vicinity of the absorption edge. All absorption denoted α_1 in Fig.16 was believed to be due to indirect transitions

Figure 16 ; A simplified absorption curve for Cu_2O where absorption to $n=1$ and $n=2$ is denoted α_1 and α_2 respectively. Temperature is 77°K .



to the $n=1$ exciton level of the yellow series with the absorption or emission of a single phonon of frequency 105 cm^{-1} . Thus, as discussed earlier, α_1 is the dominant absorption process in the range of interest for luminescence with the exception of (a) the small superimposed peak at 0.5795μ which is due to direct transitions to the $n=2$ exciton of the yellow series and (b) the constant background absorption seen at wavelengths greater than 0.62μ . This latter absorption is reported to be of different magnitude by different authors (Baumeister (1961), Gross and Pastrnyak (1959)), and we shall consider it to be negligible for the purpose of this thesis.

It will be seen later that this assumption is valid for most wavelengths of interest but as might be expected, the approximation makes results deduced from the luminescence data unreliable in the range 0.61 to 0.62μ where α_1 is small. It is also important to note that Fig.16 shows only absorption for indirect processes to $n=1$ and direct processes to $n=2$; the more detailed plot of α versus λ in Fig.12, of course, shows also the structure of the $n=2$ line asymmetry, the higher exciton levels, and the weak $n=1$ direct transition line.

For the present, we shall consider only the

overall curve shapes and we shall discuss the $n=2$ size effect in the following chapter.

The number ΔN of excitons created per unit time in a volume $A\Delta x$ at a depth x in the sample, where x is measured in the direction of propagation of light (see Fig.17) and where A is the area of the sample on which the light is incident, is given by

$$\Delta N = A\eta\sigma I_0 e^{-\alpha x} \Delta x \quad 6)$$

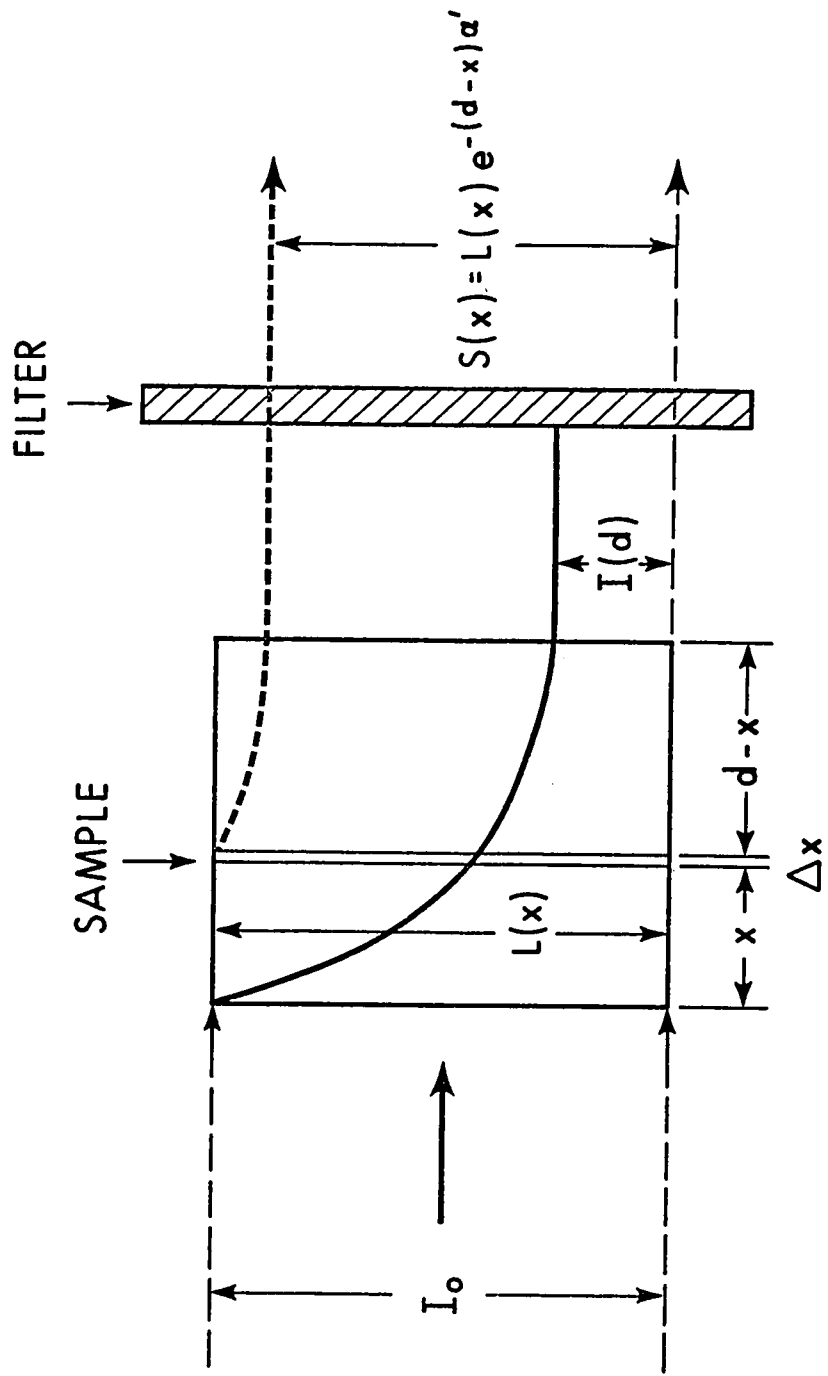
where σ is an absorption cross-section, η is the number of lattice sites per unit volume, and I_0 is defined as the number of photons of energy $h\nu_1$ per unit area per unit time entering at the surface of the sample. For our case, where the absorption is almost exclusively to excitons we have $\eta\sigma = \alpha$, which according to absorption theory is α_1 except for the contribution α_2 which we will ignore for this part of the analysis.

The expression for ΔN is then given by

$$\Delta N = A \alpha_1 I_0 e^{-\alpha_1 x} \Delta x \quad 7)$$

The number of luminescent photons ΔL , emitted with energy $h\nu_2$ originating in $A\Delta x$ per unit time will

Figure 17 : Diagram of sample illumination and detection arrangement. Note that the magnitudes of incident light I and luminescence L are shown schematically only.



be given by

$$\Delta L = \phi \alpha_1 A I_0 e^{-\alpha_1 x} \Delta x \quad 8)$$

where ϕ is the fraction of created excitons which are captured by the luminescent centers and subsequently produce luminescence. The quantity ϕ will be proportional to a capture cross-section for excitons and we shall show it to be strongly wavelength dependent.

The luminescence detected from $A\Delta x$ is smaller than ΔL for three reasons :

(a) there is a small absorption coefficient α' at the wavelength of luminescence

(b) at the very best, only half of the luminescence radiation will be emitted in the direction of the detector

(c) due to the high dielectric constant of the material ($\epsilon \approx 7$), a fraction of the radiation reaching the back surface will be reflected into the sample. To simplify our expression, we write for the signal strength ΔS detected due to the luminescence ΔL from $A\Delta x$

$$\Delta S = \phi \alpha_1 AB I_0 e^{-\alpha_1 x} e^{-\alpha_1'(d-x)} \Delta x \quad 9)$$

where the constant B takes into account the reflection and directional losses discussed above, the quantum efficiency of the photomultiplier at the wavelength of the luminescence and the transmission characteristics of the infrared filter. It is assumed that B is independent of wavelength of incident light. The inclusion of the term for the self-absorption represents a small correction to the expression but it is important for the case of a thick sample where the emitted light must penetrate through the full thickness of the sample.

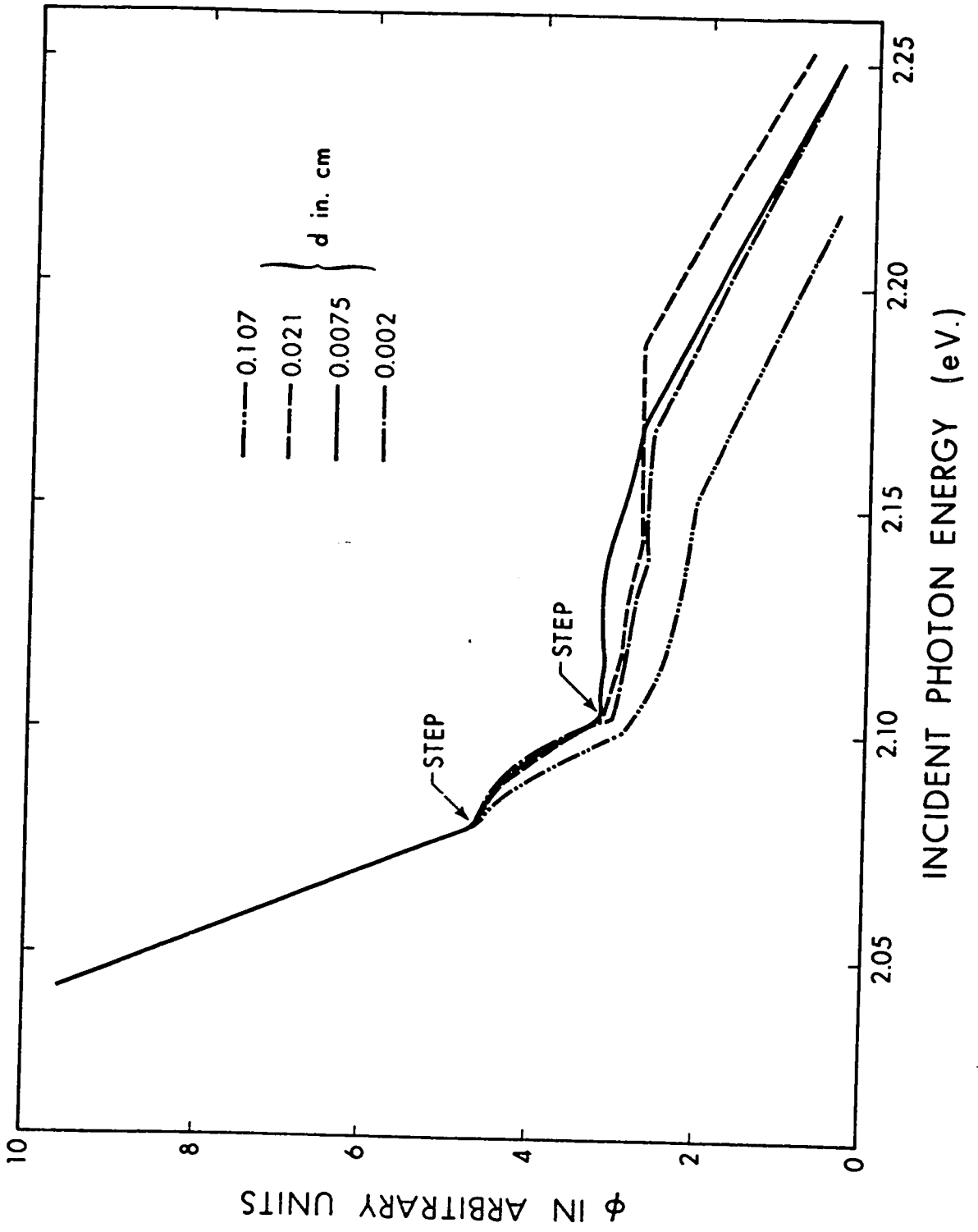
The expression for the signal detected from the whole sample of thickness d is now

$$S(d) = \phi \alpha_1 AB I_0 \frac{e^{-\alpha' d} - e^{-\alpha_1 d}}{(\alpha_1 - \alpha')} \quad 10)$$

By inserting experimental data for S and d together with the known dependence of α_1 on λ , we can compute ϕ vs. λ . It is more interesting however to plot ϕ versus the energy of incident photons as in Fig.18. Here the results for four sample thicknesses, d = 0.107, 0.021, 0.0075, and 0.002 cm (for a sample similar to that of Fig.15) are shown and although drawn from luminescence excitation curves of widely different shapes, show a very good agreement.

Two straight lines are seen of the form

Figure 18 : A plot of ϕ versus energy of incident light for four sample thicknesses.

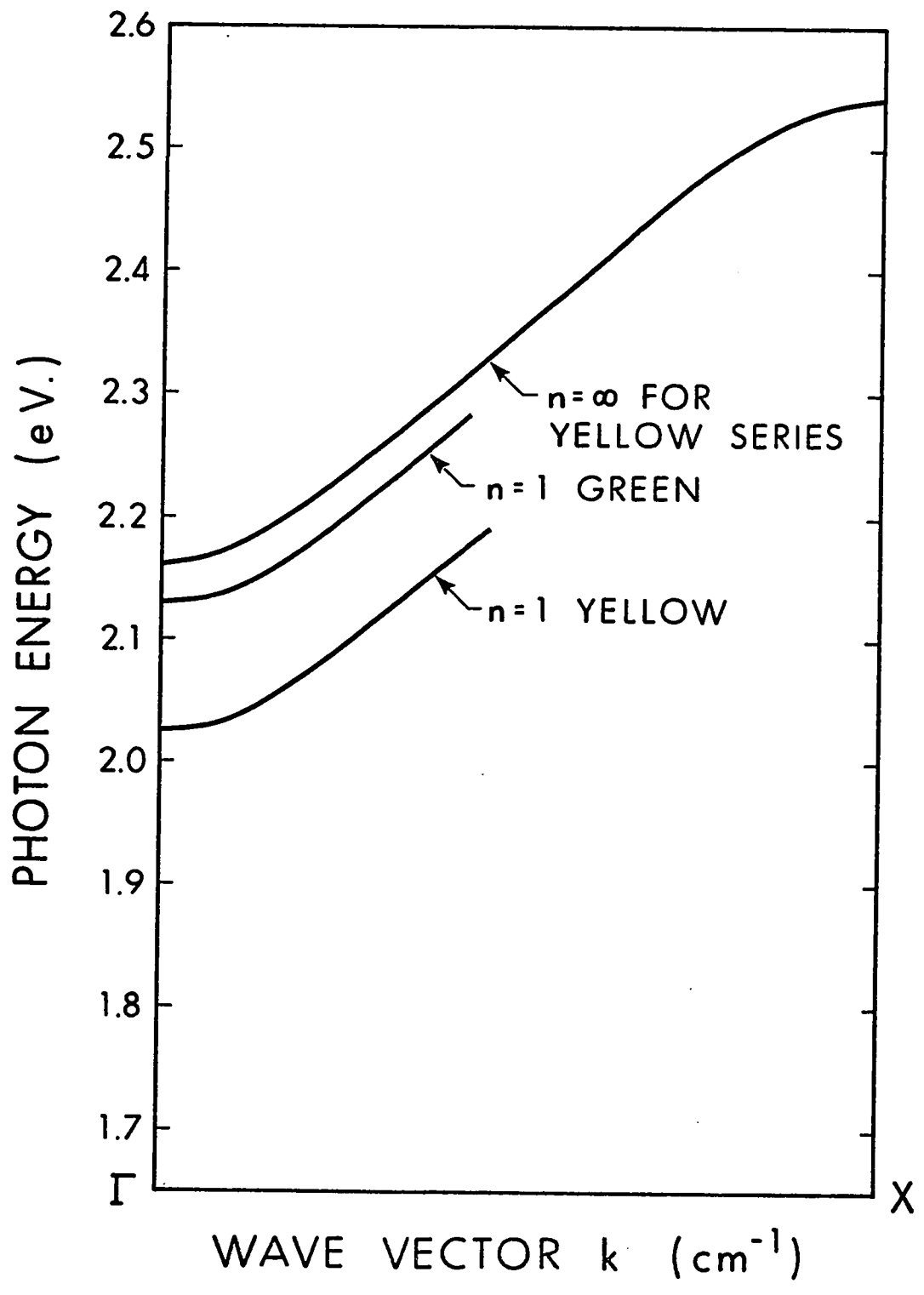


$$\phi = C - D hv_i \quad 11)$$

where hv_i is the energy of the incident light quantum and C and D are constants. Further, two well-defined steps can be seen at about $hv_i = 2.08$ and 2.105 eV. For $hv_i < 2.04$ eV the computation for ϕ becomes unreliable due to the uncertainty in the absorption coefficient for $\lambda > 0.61\mu$, as discussed earlier.

For an interpretation of the ϕ vs. hv_i results, we must go back to the absorption processes. Over a considerable range of incident photon energy, we create the $n=1$ exciton of the yellow series. The step on the absorption edge at $\lambda = 0.61\mu$ is known to be due to the onset of transitions to $n=1$ with the emission of a single 105 cm^{-1} phonon. If this phonon is the only possible one, then for $\lambda < 0.61\mu$, the created exciton must have a certain initial kinetic energy (from energy conservation considerations). Returning to the band scheme for Cu_2O and assuming that the dispersion curves for excitons follow the shape of the conduction band, we may draw the approximate scheme for exciton states in Fig.19. The proposed $n=1$ of the green series in Fig.19 is, of course, associated with the lower band of the spin-orbit split valence

Figure 19 : Approximate dispersion curves for excitons. Note that the curves shown are drawn relative to incident photon energy and have no direct relation to the band scheme for Cu_2O .



band and would not appear on a rigorous band scheme in the position indicated.

We interpret the straight line region of ϕ vs. $h\nu_i$ in the range $h\nu_i = 2.04$ to 2.08 eV as a reduction in the capture cross-section for $n=1$ excitons of the yellow series by the luminescent center as the kinetic energy of the excitons increases. The linear relationship 11) also holds for kinetic energy since this is simply given by $E = (h\nu_i - h\nu_0)$ where $h\nu_0$ is the energy for the onset of the phonon emission process.

The two steps in ϕ at $h\nu_i = 2.08$ and 2.105 eV are strongly reminiscent of the steps seen on the absorption edge for the indirect transitions to $n=1$ of the yellow series. These steps, together with the structure in ϕ which departs from the initial straight line and develops into a second line of different slope, suggests the onset of a second excitation and capture process. The frequency separation of the two steps is about 200 cm^{-1} and this leads us to propose that we are detecting indirect excitations to the $n=1$ exciton level of the green series, with absorption and emission of the 105 cm^{-1} phonon.

The second straight line region is therefore due to a relationship similar to that for $n=1$ excitons

of the yellow series.

It is most interesting that the luminescence was able to show structure due to the $n=1$ exciton of the green series. This exciton had not previously been observed in absorption or other optical effects. The optical absorption to this exciton must of course be weak in that it has not been detected in absorption measurements. However, if we say that the absorption to $n=1$ of the green series should be of the same order of magnitude as for the corresponding range of the yellow series, we can see from Fig.16 that two steps showing an increase in absorption of only 5 or 6 cm^{-1} at about 0.59μ , where the overall absorption coefficient is now about 100 cm^{-1} (and increasing rapidly), might not have been detected as significant in an absorption curve. In short, the exact magnitude of the absorption constant for absorption to $n=1$ of the green series is not known, but could be as high as that for $n=1$ of the yellow series for a region of similar excitation mechanism without having been detected in previous absorption work.

It is also interesting to note that the $\underline{K}=0$ energy of the $n=1$ exciton of the green series, measured as being midway between the two steps in ϕ in Fig.18, is at $2.093 (\pm .003) \text{ eV}$ while the Rydberg

formula for $n=2,3,4,5$ excitons predicts an energy of 2.14 eV at 77°K (Nikitine et al. (1955), Grun (1962)). The exciton is thus seen to be shifted to lower energy in a similar way to the $n=1$ of the yellow series but by a different amount. The departure from the static dielectric constant can be calculated from the Rydberg formula. This gives $\epsilon_0/\epsilon = 1.28$, where ϵ_0 and ϵ are the static and observed dielectric constants respectively, which compares to 1.15 for the analogous quantity for $n=1$ of the yellow series. Thus as we go from the lower energy yellow to the higher energy green series, the departure from the static dielectric constant for $n=1$ increases.

The straight line relationships of negative slope found for ϕ versus energy are very interesting in that the capture cross-sections are reduced with increasing kinetic energy of the excitons. It should be realised, however, that the quantity ϕ , although proportional to the capture cross-section for the excitons by the luminescent center, also contains information on the exciton lifetime dependence on kinetic energy for scattering out of the exciton states by processes other than luminescence. In particular, for the case we have been studying of low efficiency samples, the luminescence represents

at best 0.1% of the decaying excitons. It is therefore not clear at this point whether the capture cross-sections themselves are responsible for the ϕ vs. $h\nu_1$ dependence or a combination of this with the exciton lifetime dependence on kinetic energy due to some other decay process.

We may say however that the supposition that is often made in exciton theory that excitons created high in the exciton band "thermalise" in a time negligibly short is clearly erroneous in this case. If these excitons did thermalise their subsequent luminescence characteristics should be independent of the initial states, which of course is not what has been observed here.

The relative slope between the two straight lines in Fig.18 corresponding to $n=1$ yellow and $n=1$ green regions is not reliable since the absorption coefficient for transitions to $n=1$ of the green series is not known, as has been discussed above, and we therefore draw no conclusions from the slope ratio.

Conclusion to Chapter 6 : In this chapter, experimental measurements on weakly emitting samples were reported for an improved detection system.

Further exciton structure corresponding to the weak $n=1$ line of the yellow series and the $n=2,3$ lines of the green series was observed together with a new size effect in Cu_2O , whereby the $n=2$ dip of the yellow series could be made to invert to a peak on reducing the sample thickness.

An analysis was made of the overall excitation curve shape and a quantity ϕ calculated which is proportional to a capture cross-section for excitons. Curves of ϕ vs. λ indicated the presence of transitions to the previously unobserved $n=1$ exciton states of the green series.

We will go on in the next chapter to discuss in detail the size effect results.

CHAPTER 7.

Exciton Size Effect in Luminescence.

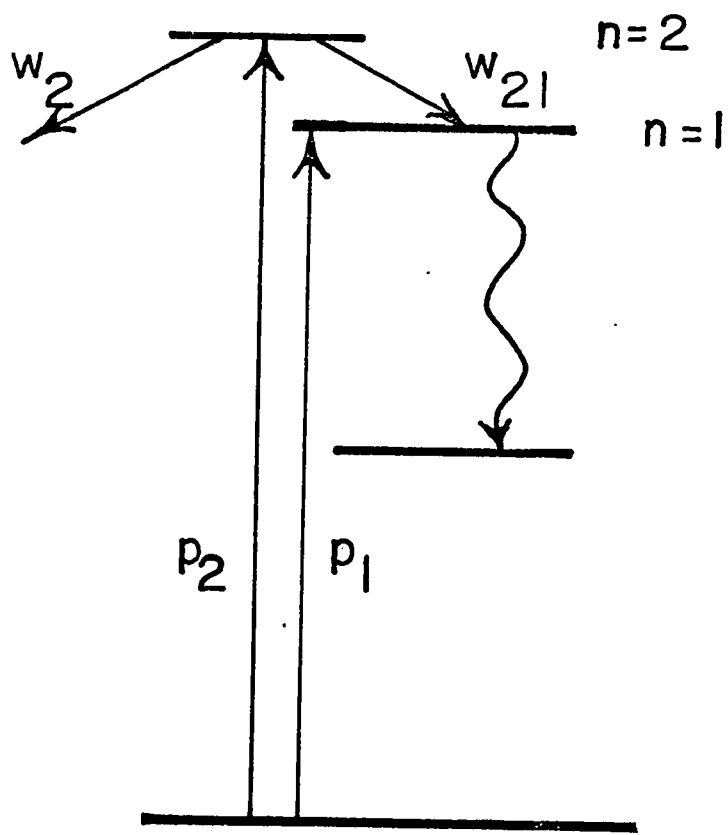
The size effect for the structure of the $n=2$ exciton of the yellow series seen in Figs.15a, 15b, and 15c can yield some interesting information on the relative probability of decays to the $n=1$ level and decays by all other processes out of the $n=2$ exciton states if we make the assumption that only $n=1$ excitons (both yellow and green) are captured by the luminescent centers. The justification for this is the good agreement found earlier for the exciton line asymmetry problem and the further evidence in the preceding chapter that the luminescence is strongly associated with the $n=1$ levels.

We can set up a simple four level system for luminescence as shown in Fig.20, and by solving for dynamic equilibrium in the usual way (see for example Di Bartolo (1968)), it can be shown that

$$L \propto p_1 + \frac{w_{21}}{w_{21} + w_2} p_2 \quad 12)$$

where p_1 is the total probability per unit time of transitions to $n=1$, p_2 is the total probability per

Figure 20 : Model for excitation and decay processes for the $n=2$ exciton of the yellow series.



unit time of transitions to $n=2$, L is the number of luminescent photons emitted per unit time, w_{21} is the probability per unit time of decays from $n=2$ to $n=1$, and w_2 is the probability per unit time of decay from $n=2$ by all other processes. The assumptions made in deriving expression 12) are

(a) that we are working with low incident light intensity, which is consistent with the experimental conditions, and

(b) that the lifetime of the luminescent center once the exciton is captured, is short, which is consistent with the lifetime measurements given in Chapter 2 and by Karkhanin and Vorob'ev (1962).

Our expression for the signal detected from $A\Delta x$ therefore becomes

$$\Delta S' = A I_0 B \left\{ \phi \alpha_1 + \frac{w_{21}}{w_{21} + w_2} \alpha_2 \phi^1 \right\} \cdot e^{-(\alpha_1 + \alpha_2)x} \cdot e^{-\alpha'(d-x)} \Delta x \quad 13)$$

where p_1 and p_2 of expression 12) have been set equal to $\alpha_1 I(x)$ and $\alpha_2 I(x)$ respectively. Also in expression 13), ϕ' is the value of ϕ for the $n=1$ excitons created by the transition $n=2$ to $n=1$. There are two possible modes of decay :

(a) involving the emission of one or more phonons

and transferring the $n=2$ excitons to an $n=1$ at some wavevector \underline{k} and

(b) a simple hydrogenic $2p \rightarrow 1s$ decay with the emission of an infrared quantum. The first process should produce excitons with less kinetic energy than that of the $n=1$ excitons created by process α_1 at this wavelength, while the second process creates excitons which are essentially at $\underline{k} = 0$. We have at present no way of distinguishing which process is dominant, but in either case we may assign $\phi' \approx 2\phi$ with a maximum error of 50%. (For this estimate, we compare the dispersion curves for excitons and the ϕ dependence for $n=1$ of the yellow in the same energy range.) The overall expression then becomes

$$S' = A I_0 B \phi \left\{ \alpha_1 + \frac{w_{21}}{w_{21} + w_2} 2\alpha_2 \right\} \cdot \frac{e^{-\alpha' d} - e^{-(\alpha_1 + \alpha_2) d}}{\alpha_1 + \alpha_2 - \alpha'} \quad (14)$$

In principle, by fitting expression 14) to any experimental curve of S vs. λ , the ratio $w_2:w_{21}$ could be computed. However, the most convenient method for a determination of $w_2:w_{21}$ is to measure the sample thickness for which neither a dip nor a peak is produced at the $n=2$ wavelength, ie, the curve is smooth. But such a smooth curve is exactly the result one would obtain when no

p_2 process is present at all, which is the expression obtained for S in the preceding chapter. By calculating $S' - S$ for the wavelength of the $n=2$ line and setting this equal to zero, the ratio $w_2:w_{21}$ can be computed by iterative methods (see Appendix B).

Using the data from Fig.15b, the thickness $d=0.0045$ cm produced such a smooth curve giving $w_2:w_{21} = 9(\pm 4):1$ ie. at the temperature of 77°K , the decay from $n=2$ to $n=1$ is about a factor of ten less probable than the scattering out of $n=2$ by all other processes (the uncertainty in $w_2:w_{21}$ arises due to the uncertainty in ϕ'). A plot of the $w_2:w_{21}$ ratio solutions for various sample thicknesses is shown in Fig.21, and it is clearly seen that if the thickness at which a smooth curve was found had been in the range $d < 0.002$ or $d > 0.02$ cm, then a determination of $w_2:w_{21}$ would have been considerably more difficult.

To illustrate the effect of this ratio, some computed curves for S' (using an averaged value of ϕ vs. λ) for a thickness $d = 0.002$ are shown in Fig.22 for $w_2:w_{21}$ ratios of 10, 25 and 50:1.

The mechanisms involved in luminescence are now fairly clear, in short, an exciton may be captured at a luminescent center, producing in effect an excited state of the center which, in turn, decays

Figure 21 : Plot of the ratio $w_2:w_{21}$ for the various sample thicknesses required to produce a smooth curve in luminescence.

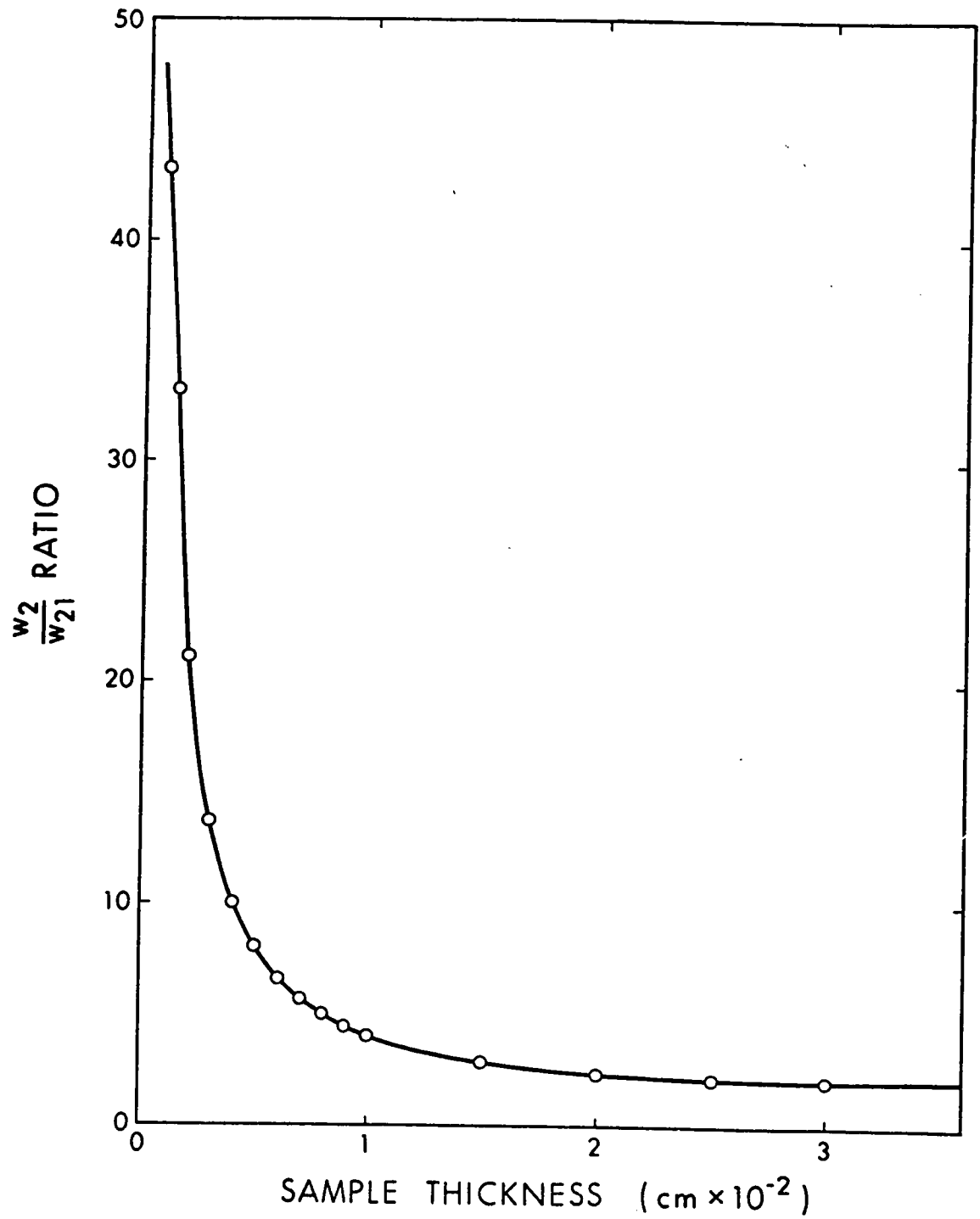
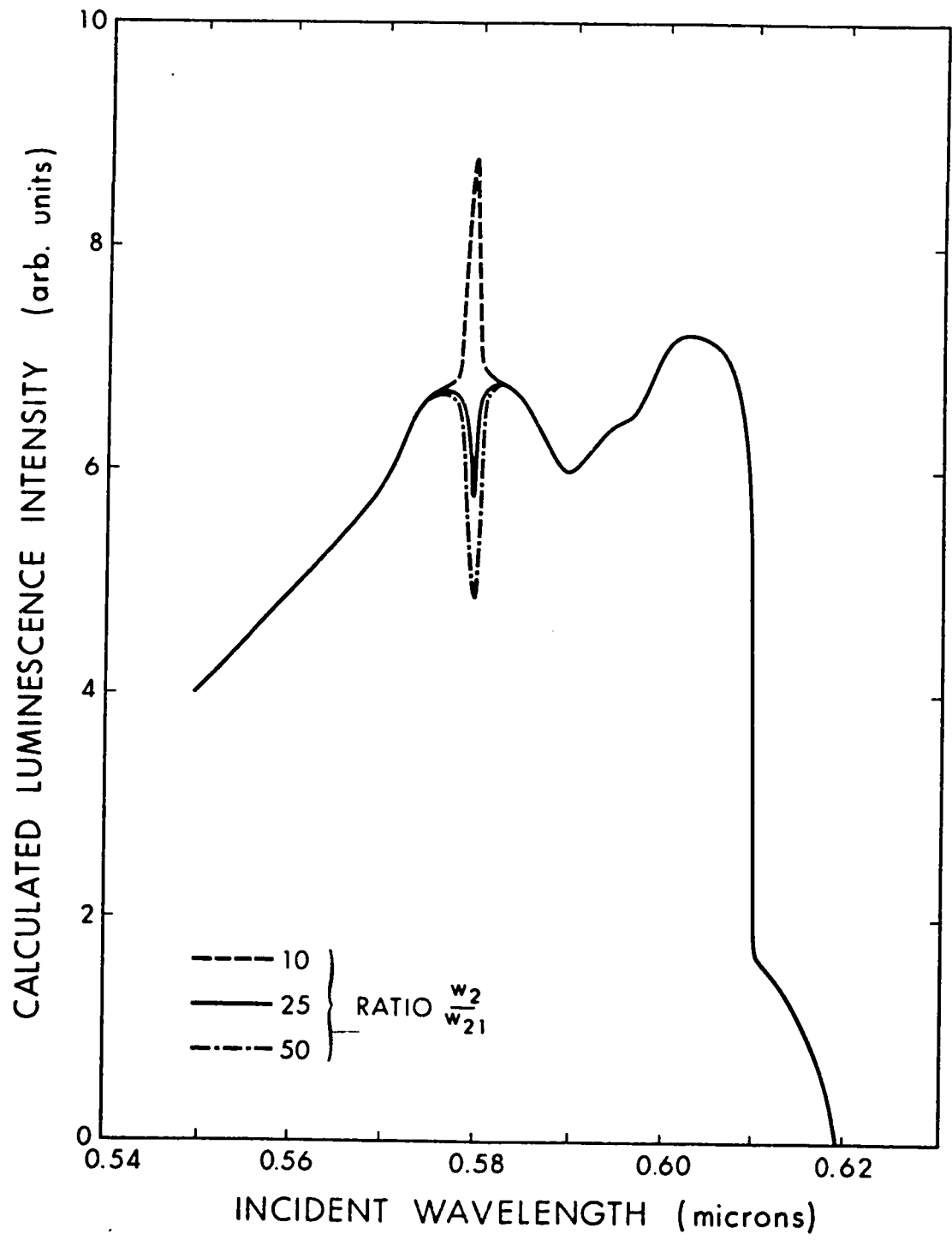


Figure 22 : Calculated luminescence excitation curve for a sample thickness of 0.002 cm. The effect of the $w_2:w_{21}$ ratio is shown for the three values 10:1, 25:1, and 50:1.



radiatively with a large Stokes shift. This is consistent with the configuration co-ordinate model for a luminescent center. That the excitons most likely to be captured are those with $n=1$ is intuitively reasonable in that $n=1$ excitons have a Bohr radius of only a few atomic dimensions ($\sim 5\text{\AA}$) and thus interactions with a lattice defect are strong. For excitons of $n=2$ and higher, the exciton wave functions extend over a large number of lattice sites (Bohr radius $\sim 50\text{\AA}$), and interactions with a single lattice vacancy are expected to be weak.

Conclusion to Chapter 7 : The size effect associated with the $n=2$ exciton structure of the yellow series has been analysed on the basis of a model whereby the infrared luminescence represents a decay from an $n=1$ exciton level only. In this way, we were able to calculate a value for the decay probability from $n=2$ to $n=1$ of the yellow series relative to decays out of $n=2$ by all other processes.

CHAPTER 8.

The Luminescent Center and Electron Paramagnetic Resonance.

This far we have avoided specific mention of the nature of the luminescent center, although the characteristics of this entity have been encountered in all aspects of the present study. To recapitulate some of these, we have seen :

(a) that the response time of the luminescence was fast, with $\tau \leq 10^{-7}$ sec. which means that the process of excitation of an exciton, capture by a center, and subsequent radiative decay, can all occur within this period of time,

(b) the temperature dependence of the luminescent intensity indicates that the center may be thermally populated by electrons and when so populated, the center is not available for luminescence,

(c) the non linearity of the luminescent intensity with intensity of incident light for high incident photon fluxes, suggests that the lower level of the decay transition at the luminescent center has a relatively long lifetime (compared to the response time above),

(d) the center is extrinsic to the ideal Cu_2O

lattice and since it can be removed on re-heating the sample under high vacuum conditions, we conclude that it is most probably of point defect character.

This latter view was also supported by the electroluminescence studies of Frerichs and Lieberman (1961) who concluded that the μ infrared luminescence takes place at Cu^+ vacancies. Such a center would fit the experimental results outlined so far but since the preparation condition mechanisms for producing a luminescing sample are still poorly understood, we cannot say for certain from the present work that this is the luminescent center.

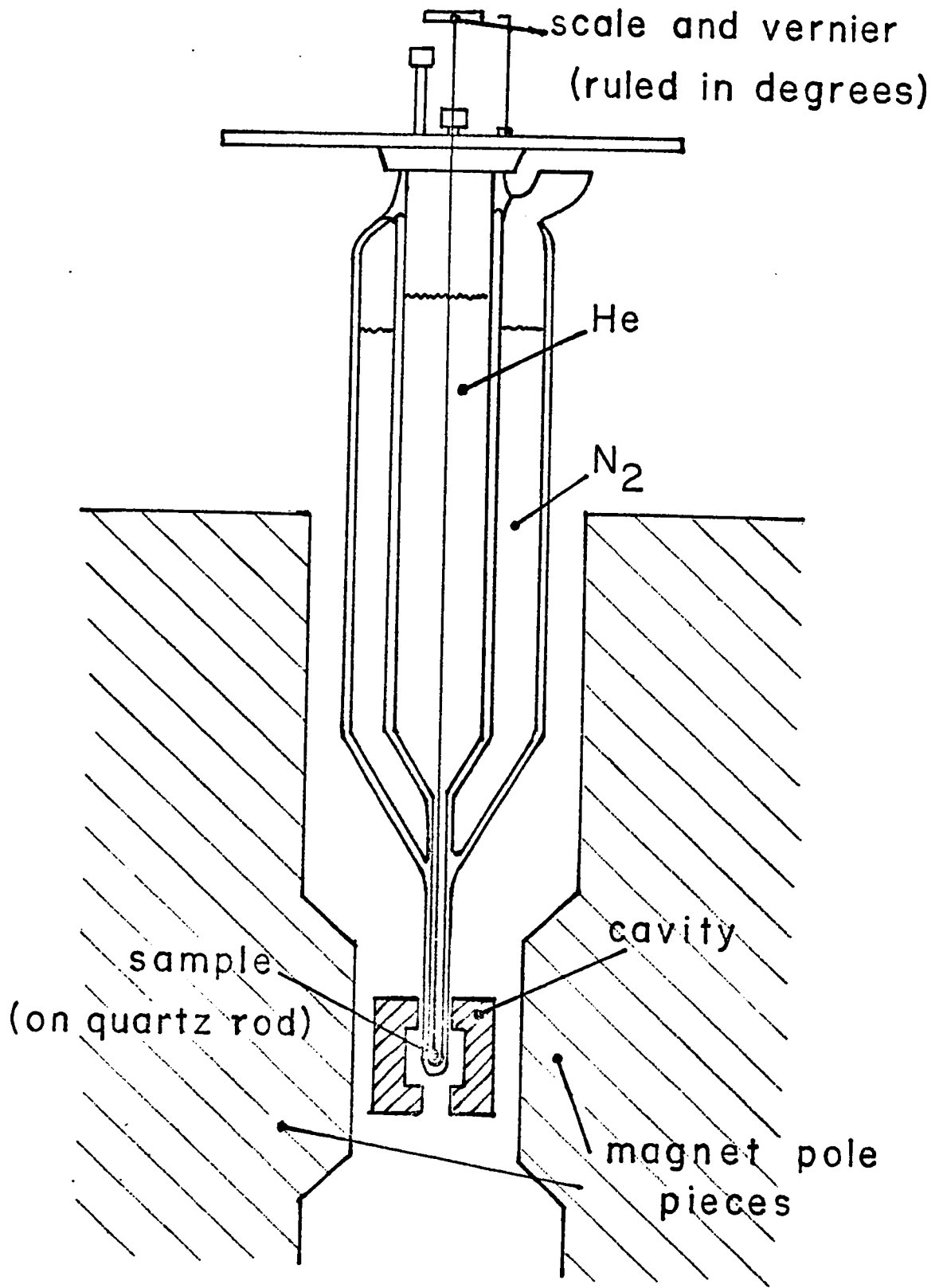
In an attempt to identify the nature of the center, an e.p.r. study was made of our samples. This technique had already been shown to be a valuable tool in the study of impurity states in other semiconducting materials (England and Schneider (1951), Portis et al. (1953), and a review by Lancaster (1967)) and it was hoped that useful information on Cu_2O could be obtained. No e.p.r. spectra had been published up to the present (with the sole exception of a reference in a paper by O'Keeffe et al. (1963) of a signal in neutron irradiated material). It was found for our samples that it was necessary to go to 4.2°K before a measurable signal could be obtained.

The cryostat used for this purpose is shown in Fig.23 and, in brief, it consisted of a double Pyrex dewar with a quartz helium tip which was designed to fit inside a standard e.p.r.cavity. The cryostat was mounted with the dewar tip and the cavity between the magnet pole pieces of a Varian model - V4500 spectrometer. The microwave frequency used was 9.386×10^9 Hz and the sample to be measured was mounted on a thin quartz rod, suspended in the liquid helium inside the cavity. The magnetic field was modulated at 100 KHz.

For this experiment, where we were seeking information on the luminescent center, it was decided that the e.p.r. measurements should be made on a number of samples whose other physical properties of interest had already been measured, allowing correlations to be made between these properties and the e.p.r. signals.

Thus six single crystals were cut from the same starting material and then treated individually under various temperature and vacuum conditions in the system of Fig.6, to change the sample composition in a known way. The conductivity of the samples was monitored as they were cooled and the activation energy E calculated from the formula

Figure 23 : The e.p.r. Helium cryostat.
The system was arranged such that the microwave cavity
could be adjusted into position without disturbing
the dewar.



$$\sigma = \sigma_0 e^{-E/kT} \quad 15)$$

where σ is the conductivity and σ_0 is a constant. Fig.24 shows the cool-down plot of $\log \sigma$ vs. $1/T$ for the six samples (A,B,C,D,E, and F).

The photoconductivity of the samples was then measured with the sample in situ in the quartz tube of Fig.6, again A.C. techniques were used with a lock-in amplifier for detection. The photoconductivity excitation curves for the six samples at room temperature are shown in Fig.25.

The samples were removed from the quartz tube after the heat treatment and photoconductivity measurements, and their luminescence properties measured in the cryostat of Fig.14. The luminescence results for the six samples are shown in Fig.26.

The sample treatment histories are summarised in Table 1 and, in brief, they were as follows :

Sample A : Natural surface heated in vacuo to 700°C for 1h and then gradually cooled over 24h with a pressure decreasing from 1×10^{-6} torr at 700°C to 1×10^{-7} torr at 20°C. The resulting activation energy was 0.35 eV at room temperature. The conductivity curve upon cooling is shown at curve A, Fig.24.

Figure 24 : Plot of $\log_{10}\sigma$ vs. $1/T$ on the cool-down process for the six samples A,B,C,D,E, and F.

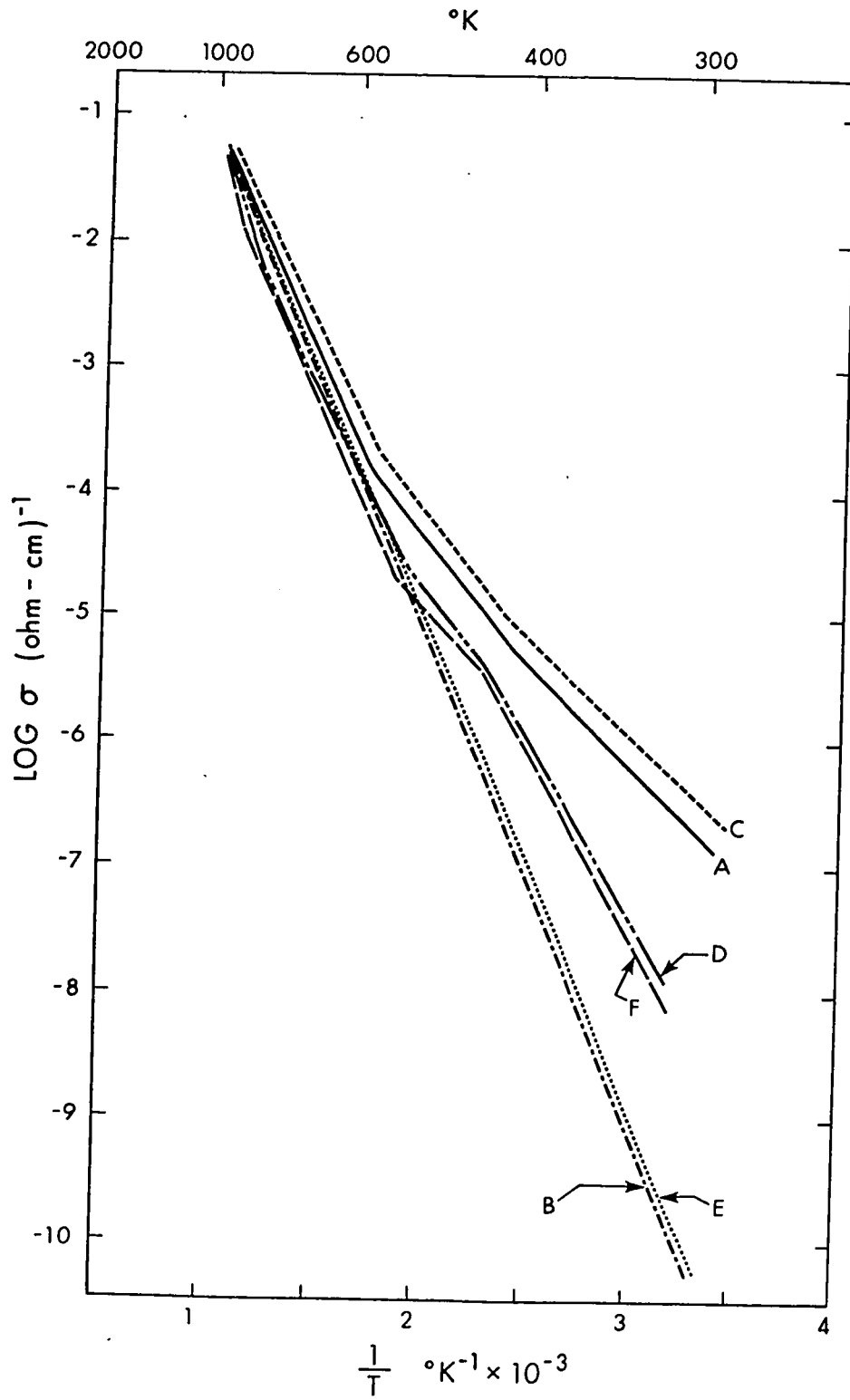
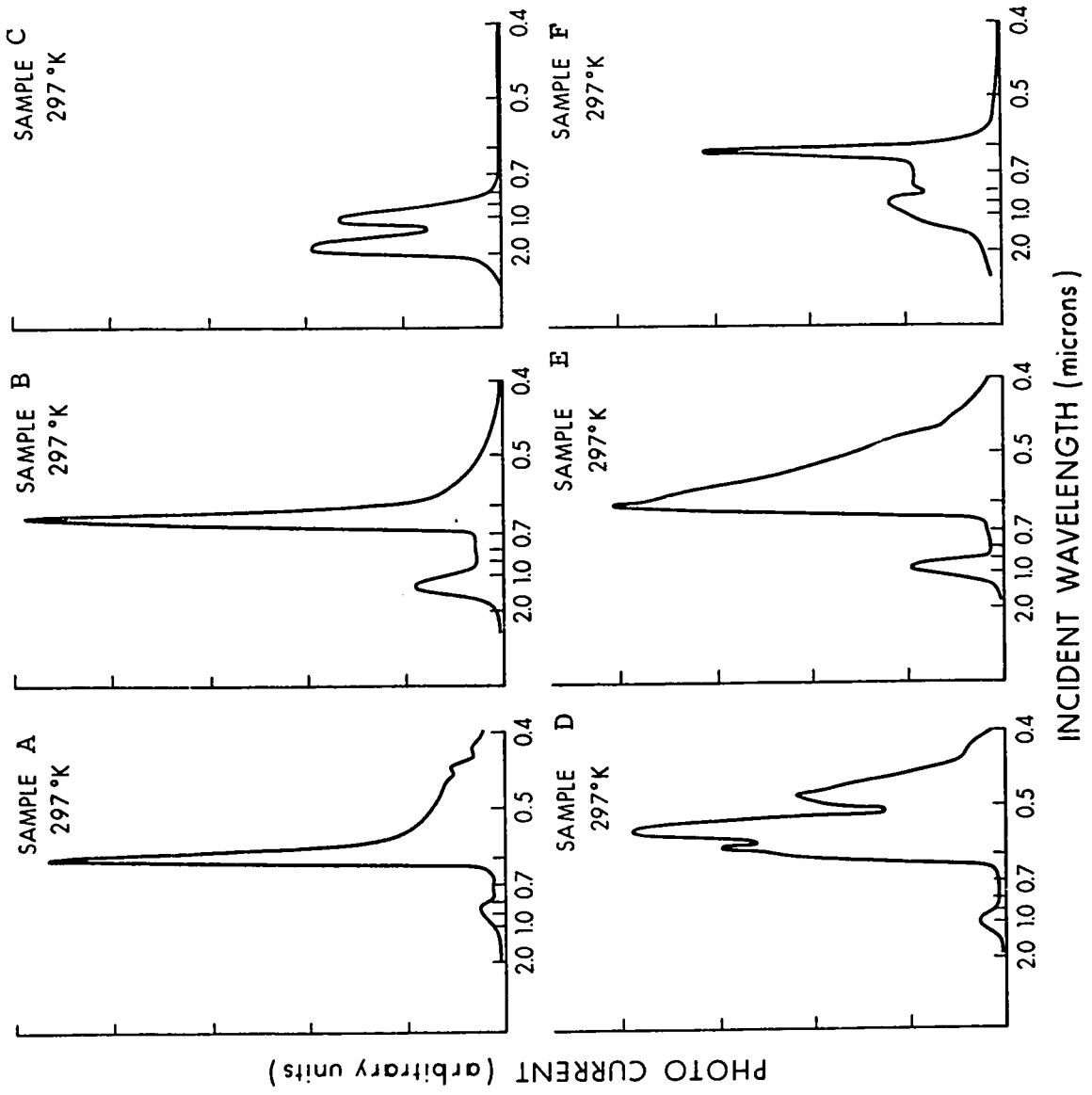


Figure 25 : Photoconductivity excitation curves for the samples A,B,C,D,E, and F at 300°K.






Figure 26 : Luminescence excitation curves for samples A,B,D,E, and F at 77°K. Sample C showed no detectable luminescence.

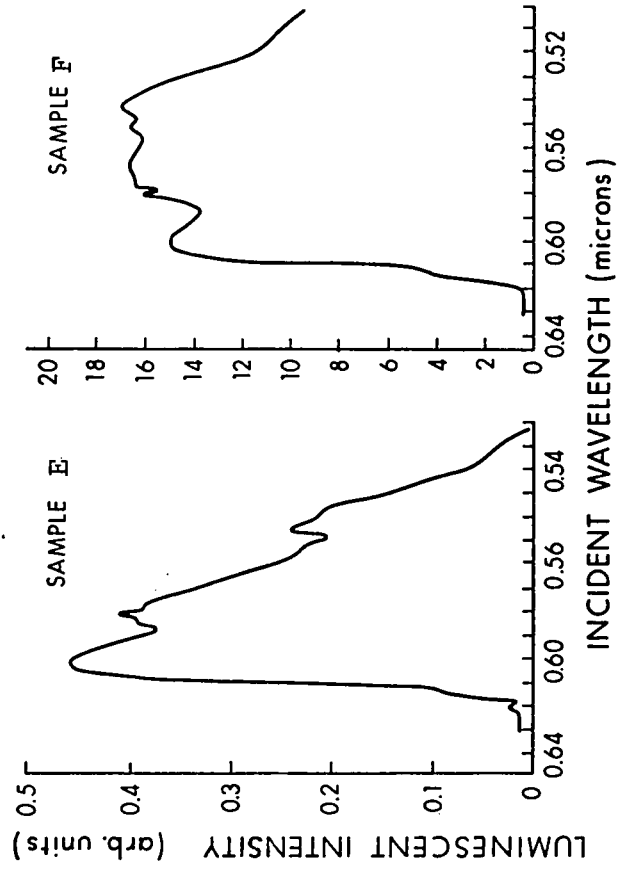
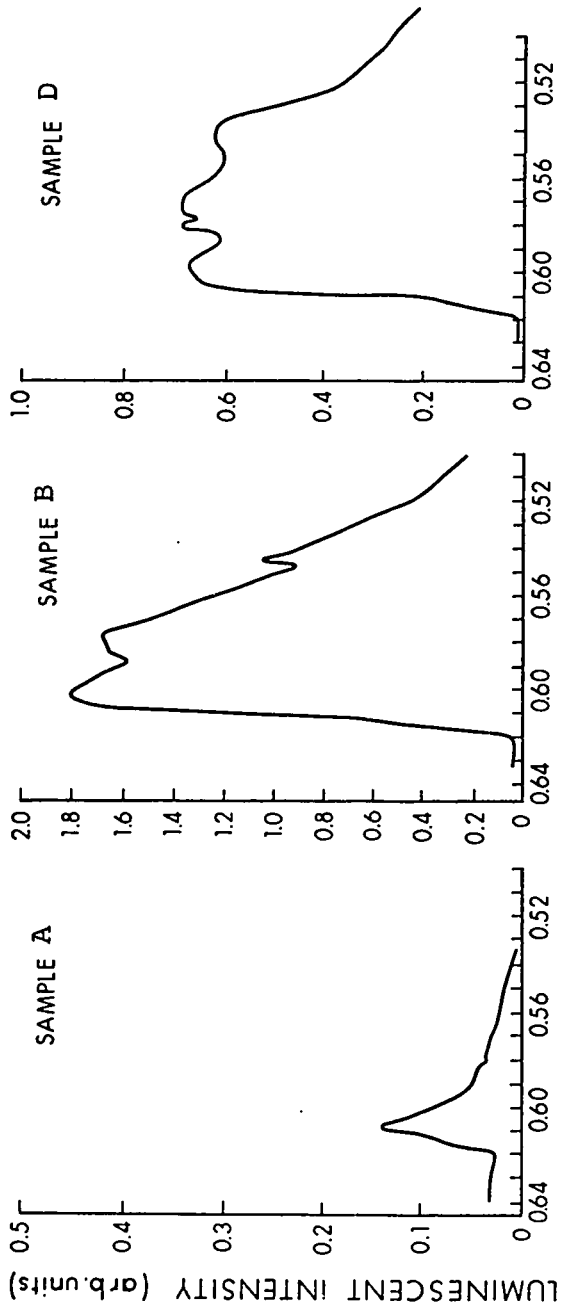


Table 1 : Summary of sample treatment history, activation energies, photoconductivity and luminescence properties.

SAMPLE	COOL-DOWN CONDITIONS	PHOTO- CONDUCTIVITY MAXIMA	LUMINESCENCE	E.P.R.	ACTIVATION ENERGY	SURFACE
A	10^{-6} to 10^{-7} below 700°C	0.6, 0.9 μ	"Weak"	Complex with 45 and 600 symmetries	0.35eV	natural
B	10^{-7} below 800°C	0.62, 1.3 μ	"intermediate"	2 lines, orienta- tion independent	0.78eV	ground
C	air from 1000°C	1.0, 1.8 μ	undetectable	complex, with 45 and 600 symmetries	0.31eV	ground
D	3×10^{-4} from 1000°C	0.48, 0.54 0.6, 1.0 μ	"intermediate"	2 lines, orienta- tion independent	0.53eV	ground
E	10^{-7} below 800°C	0.6, 1.0 μ	"intermediate"	2 lines, orienta- tion independent	0.76eV	ground
F	2×10^{-7} from 800°C in presence of Cu metal	0.61, 0.9 μ	"strong"	2 lines, orienta- tion independent	0.56eV	ground

Samples B and E : These were each individually heated to 1000°C and gradually cooled to room temperature over a period of 48h. At 800°C, the vacuum was 4×10^{-7} torr and improved further during cooling. The sample surfaces were ground prior to heating (curves B and E, Fig.24).

Sample C : Ground surface. The sample was heated to 1000°C and allowed to cool gradually in air at atmospheric pressure over 48h. The surface was again as shiny as is characteristic of natural crystals. The conductivity curve is shown at curve C, Fig.24. (Note : Here "natural" refers to crystals grown in the usual way in our laboratory.)

Sample D : Ground surface. As for samples B,C,E, and F, it was heated to 1000°C but then cooled gradually over 48h at the intermediate pressure of 3×10^{-4} torr, as obtained from a mechanical pump. A liquid nitrogen trap was used to prevent organic vapours from reaching the sample. The conductivity curve is shown as curve D, Fig.24.

Sample F : Ground surface. This sample was heated to 1000°C in the presence of a piece of copper foil, in order to reduce the available free oxygen at the sample site. It was also cooled gradually over 48h with a vacuum of 2×10^{-7} torr at 800°C. The conductivity

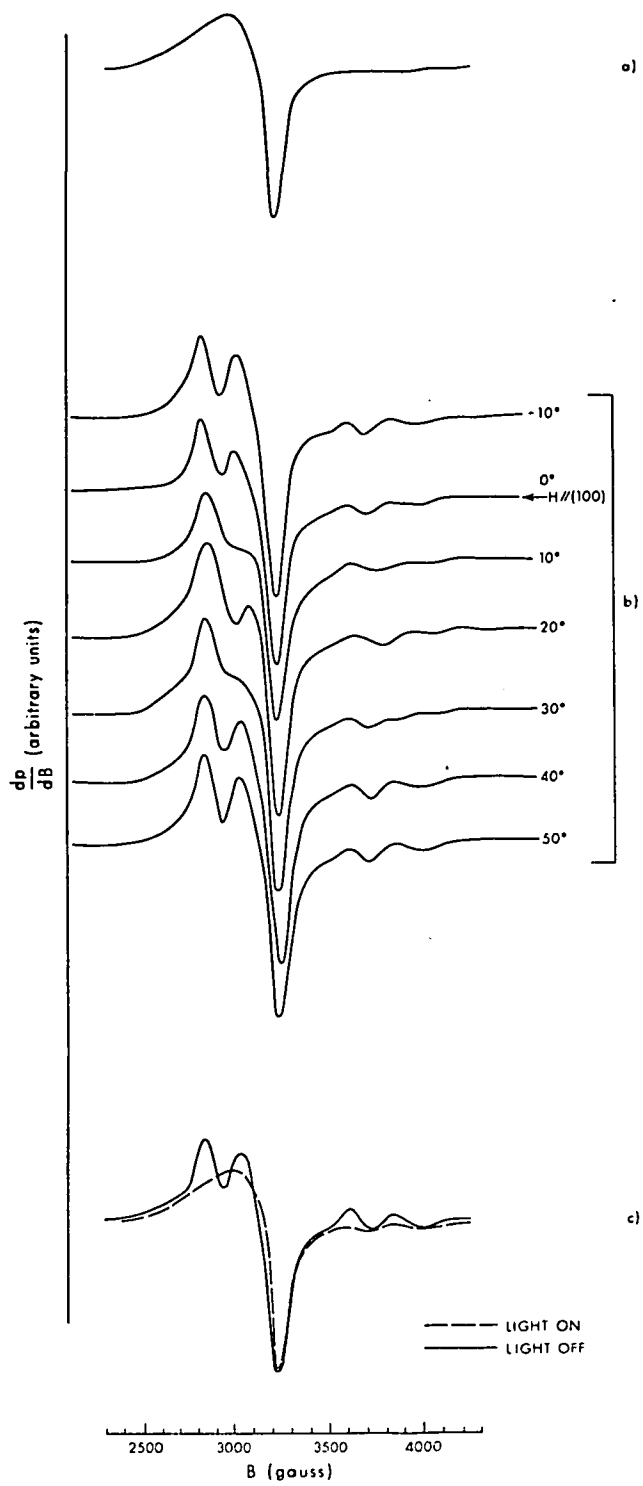
curve is plotted as curve F, Fig.24. On return to room temperature, there was no evidence of oxidation on the copper foil.

The e.p.r. spectra for the six samples fell into two distinct types which are categorised by the spectra shown in Fig.27. In Fig.27a, for samples B,D,E, and F, a single asymmetrical line was observed at 3180 gauss with a broad linewidth of ~ 200 gauss. Superimposed on this broad line there was a single sharp line of lower magnitude at 3300 gauss, linewidth ~ 5 gauss. This spectrum was found to be independent of crystal orientation for these four samples.

Samples A and C both showed a considerably more complex spectrum (Fig.27b), which consisted of both the lines observed for samples B,D,E, and F, but superimposed on these was a series of broad lines which showed a strong orientation dependence. Two strong lines of about 100 gauss width are seen at 2890 and 3080 gauss, with two weaker lines, also about 100 gauss in width, at 3600 and 3930 gauss.

The sample of Fig.27b, sample C, was mounted such that the (100) cubic crystal axis was initially parallel to the magnetic field of the magnet. It was found that the spectrum remained invariant under rotations of 45° (to (110)), and 90° (to the (010))

Figure 27 : Electron paramagnetic resonance spectra for Cu_2O at 4.2°K . Curve a) spectrum typical of samples B,D,E, and F (independent of crystal orientation); b) spectrum typical of samples A and C; c) photosensitivity of the spectrum for samples A and C. Here curves for the non-illuminated and white light illuminated samples are shown.



crystal axis). The spectrum for other rotations does not, however, interpolate in a simple way between these and there appears to be some symmetry for rotations of 60° (see Fig.27b for -10° and 50°).

The light from a zirconium arc lamp was passed through a series of interference filters for the visible and near infrared region (out to 2μ) and was then focussed on to the sample in the dewar by means of the usual irradiation window in the e.p.r. cavity. It was found that the spectrum of Fig.27a for samples B,D,E, and F was unaffected by the presence of light although the spectra for samples A and C did show some change. This response appeared to be sensitive to all wavelengths in the visible region but was not of sufficient magnitude to permit a determination of wavelength for maximum sensitivity. The effect of white light was to reduce the spectra of Fig.27b to a similar form to that of Fig. 27a (see Fig.27c), where again the spectra appeared to be independent of crystal orientation. The time constant for the process for both light on and light off was about 5 seconds.

The correlation between the complexity of the e.p.r. spectrum and the sample activation energy appears to be good (see Table 1), with the lowest activation energy samples A and C producing the most

complex spectra.

The end we set out to achieve has not, however, been fulfilled, since the luminescence excitation curve data in Fig. 26 indicates that the samples annealed under the highest vacuum conditions produced the strongest luminescence.

We have seen here that there is little direct correlation between the e.p.r. spectra and the luminescence properties of the samples, and it is clear that the center responsible for e.p.r. (As a rule, however, it appears that samples whose e.p.r. spectrum is complex, are poor emitters, thus establishing an inverse type of correlation).

The results for the sample annealed in the presence of copper, Sample F, are striking in that the overall luminescent intensity is significantly increased (by a factor of about 20) over the highest value found for samples annealed in the usual way. We have thus finalised the procedure to be adopted in order to produce such a strongly emitting sample. It is interesting to note that the excitation curve for the five samples exhibiting luminescence (sample C showed no detectable signal), fall with good agreement into the categories "strong", "weak" and "intermediate", as defined in the earlier work.

Similarly, the correlation between e.p.r. signals and photoconductivity work is poor. Also, there is little or no correlation between photoconductivity and luminescence, with the possible exception of sample C, which shows no photoconduction or luminescence sensitivity in the visible wavelength region.

For the e.p.r. results, our first inclination on observing the asymmetrical line profile of Fig.27a for samples B,D,E, and F, was to assign this to conduction electron spin resonance in copper, since it was recently shown that samples of Cu_2O grown in our usual way can contain large numbers of copper metal inclusions ranging in size from about 0.01 to 1μ (Kuzel et al. (1970)).

The line width and profile is not, however, consistent with those observed for other metals (Feher and Kip (1955), Dyson (1955)) and further, Wertz (1955) has indicated from theoretical considerations that a resonance should not be observable in copper. Since this line and the others observed in Fig.27b are so broad and do not appear to be associated with the luminescent center, we shall not speculate further here on their origins.

Conclusion to Chapter 8: Here we have attempted to discover the nature of the luminescent center by the technique of electron paramagnetic resonance. Unfortunately, only an inverse correlation between e.p.r. results and luminescence excitation curves and intensity is found and further, no obvious correlations between e.p.r. and photoconduction appear to exist.

The useful information for luminescence gained from the experiments is in the result that samples annealed in good vacuum in the presence of a piece of copper metal produce the strongest luminescence, and similarly, samples annealed in poor vacuum do not luminesce well, if at all.

CHAPTER 9.

Conclusion.

The results for luminescence and sample treatment history found in the previous chapter, although quite definite in themselves, are nevertheless confusing in the light of the discovery of large inclusions of unoxidised copper metal discussed earlier. The number of these, and their frequency of occurrence would imply that the material is already "copper-rich", and the addition of more copper, as in the annealing process for strongly emitting samples, would have little effect.

Since this is not so, we must conclude that the chemical equilibria of Cu_2O at high temperatures are even more complex than has been believed to date, and we make no attempt here to speculate on the processes involved.

The exact nature of the luminescent center is therefore not known, although we have accumulated sufficient experimental evidence of its nature to describe adequately its physical properties. Further, we are able to produce at will samples which will luminesce using the methods described in the previous

chapter.

To summarise our model of luminescence then, we have shown that the effect is a result of the radiative decay of an $n=1$ exciton (of either the yellow or green series) which has been captured by the luminescent center. That the center is also an acceptor for electrons is shown in the temperature dependence results, and it therefore seems likely that it is the electron of the electron-hole bound pair of the exciton which is first captured by the neutral center. This capture process will involve a loss of energy, probably in the form of the localised phonons involved in polarising the lattice surrounding the center. The captured exciton-center complex is now essentially only an excited state of the center which decays radiatively to a ground state which still retains the polarisation of the lattice (Franck - Condon principle in the configuration co-ordinate model for luminescence) (Pringsheim (1949), Kallmann (1962), Goldberg (1966)). This ground state for luminescence is therefore not the ground state of the system, and it relaxes by a further emission of phonons, bringing the lattice polarisation back to the normal configuration for the unoccupied center.

These two phonon emission processes

represent the energy loss mechanism producing the large Stokes' shift.

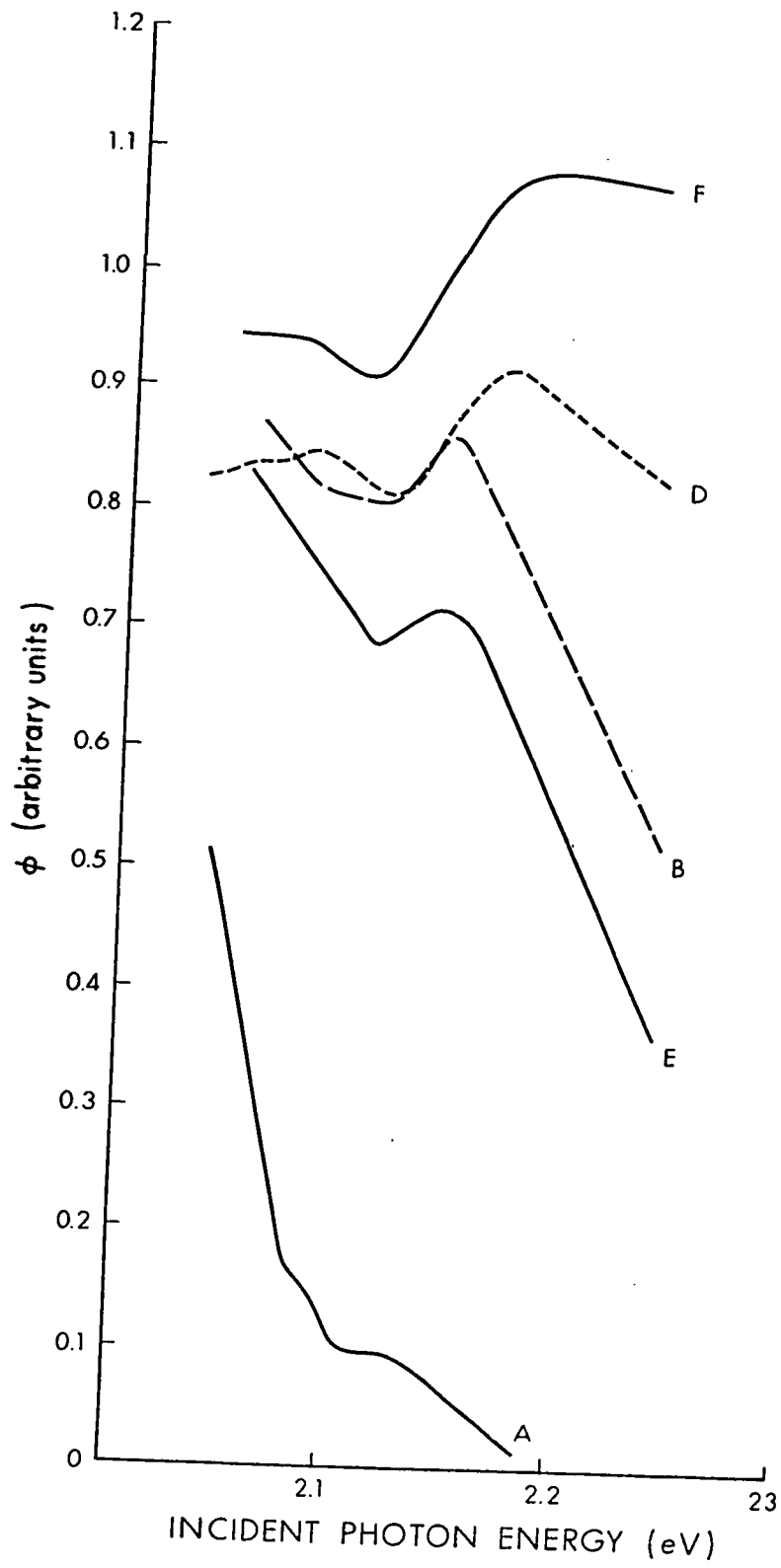
This model is also in agreement with the luminescence spectral distribution results, where a single broad peak is observed (Fig.1).

The results for the exciton capture cross-section ϕ are very interesting in that the presence of $n=1$ excitons of the green series, which had not been previously observed, was detected. Similarly, as mentioned in the introduction and in the text, the $n=2$ line asymmetry problem has been resolved. We believe that further information about the exciton lifetime dependence on wavevector K than is given here, could be derived by careful measurement of ϕ vs. λ for a number of samples over a complete range of temperatures, although this type of work is not possible with the cryostats described here.

The most suitable samples for these effects are the weak emitters, since for these, the number of excitons which undergo luminescence decay is negligible compared to the number decaying by other processes, and it is these other processes we would wish to investigate.

The ϕ vs. $h\nu_i$ curves for strongly emitting samples show ϕ to be relatively independent of wavelength (Fig.28), and we believe this effect to be due to the

Figure 28 : Plots of ϕ vs. λ for the samples A,B,D,E, and F of Fig.26. It is seen that for the weakest emitter, sample A (estimated quantum efficiency $\sim 0.05\%$), ϕ vs. λ is similar to the results given previously in Fig.18. For the strong emitters, however, (see sample F, curve F) ϕ vs. λ departs from this form.



increased concentration of centers which results in the luminescence no longer being a negligible decay process. The ϕ vs. λ results are thus only reproducible with any degree of accuracy for weak emitters (Fig.18).

The techniques used in this work of detailed study of excitation curves for luminescence correlated to known absorption processes have been shown to be of considerable value in the case of Cu_2O , since the luminescence has been seen to be an excellent probe of the excited states of the material. More work along similar lines could be performed to gain further information on the behaviour of excitons in this, the ideal exciton solid.

ADDENDUM.

Raman Effect in Cuprous Oxide Compared
to Infrared Absorption.

Introduction

There has been, to date, a marked absence of reported data on the Raman effect in Cu_2O . There are several reasons why this should be so, but primarily the difficulties have arisen from a) the presence of macroscopic light scatterers in the material and b) the position of the absorption edge at about 6400 \AA at room temperature while most available spectrometers and intense light sources operate at wavelengths shorter than this value.

It is well known that crystals of Cu_2O produced by the grain-growth method (Toth et al., 1960) contain voids of up to 0.1 mm in size, and a recent electron microscope study (Kuzel et al., 1970) has shown that over and above the presence of voids, the material contains copper inclusions ranging in size from about 0.1μ to 10μ diameter.

These two macroscopic crystal defects are responsible for the strong light scattering in the material. For the present study we were able to grow samples with a minimum of voids by careful sample preparation involving long annealing periods (20 - 30 days). These samples show excellent light transmission and are well suited for Raman work. There does remain, however, the presence of

copper inclusions since no preparation conditions have yet been found which will remove them. Scattered light from the samples is therefore still strong but is reduced to an acceptable level.

The problem of obtaining adequate light transmission has been overcome by the recent availability of strong c.w. laser lines in the region $\lambda > 6400 \text{ \AA}$. The line available to us for this investigation was Krypton 6471 \AA which, though still appreciably absorbed ($\alpha \sim 15 \text{ cm}^{-1}$) by Cu_2O , gives sufficient transmission to produce measurable Raman scattering. (Earlier reflection type measurements with He-Ne and Ar laser lines at 6328 and 4880 \AA failed to produce a detectable signal).

Experiment

The equipment was arranged for right-angle scattering measurements with incident Kr laser light (at 20 mw power) polarised perpendicular to the plane of scattering. This arrangement lends itself to a relatively straightforward analysis of Raman scattering results for cubic crystals, such as Cu_2O . Other configurations were tried but since no additional information was gained, the results reported here are for the right angle system only.

The scattered light was analysed by a Spex Model 1401 double grating spectrometer with a photomultiplier pulse counting system. The photomultiplier and detection system sensitivity can be assumed to be reasonably uniform in the frequency range of interest to us here, (100 to 700 cm^{-1} , or within 230 Å of the 6471 Å line). Further, the system was carefully checked for grating ghosts, non resonating lines from the laser discharge tube, and Raman lines from the sample supports (glass rods or glass capillary). The non resonating laser lines were attenuated by means of an interference filter peaked sharply at the laser line.

Spectra from both crushed and single crystals were measured. The crushed samples were prepared from single crystals and had particles of about 0.5 mm length. Although they were randomly oriented, they produced the strongest signals, making a higher resolution possible. For these samples we are still dealing essentially with a single crystal since the laser focus diameter is always ≤ 0.1 mm and the particles of the crushed samples were approximately 0.5 mm apart.

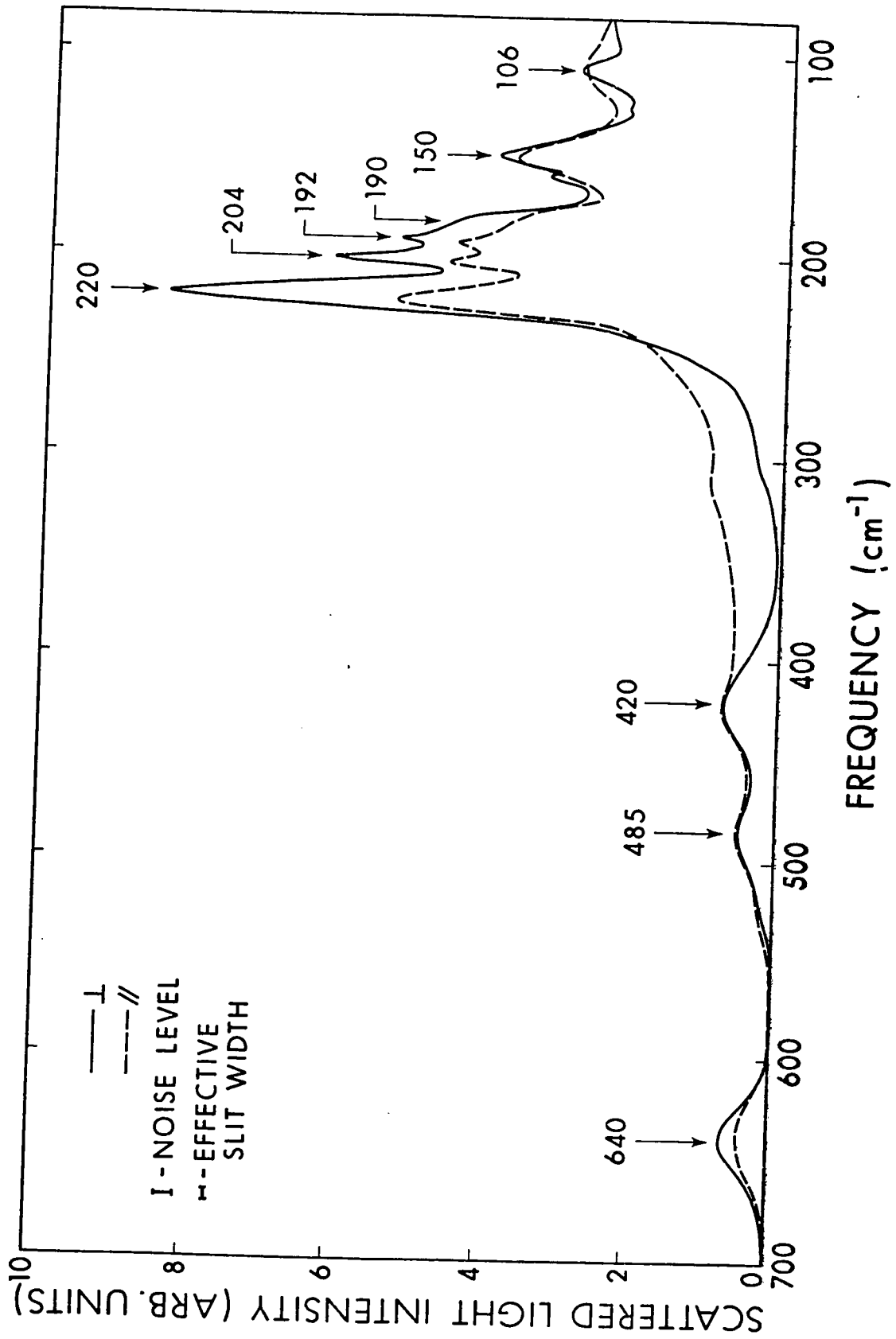
The results for a crushed sample are tabulated in Table 2 and shown in Fig.29 together with the

Table 2 : Summary of Raman and Infrared results.

Key to symbols :

$\bar{\nu}$	frequency in cm^{-1}
ρ	depolarisation ratio
a)	present work
b)	O'Keefe (1963)
c)	Pastrnyak (1959)
d)	Bouster et al. (1963)

Figure 29 : The Raman spectrum of Cu_2O for a crushed sample at 297°K . The exciting radiation is $\text{Kr. } 6471\text{\AA}$.



effective slit width (combined slit width and response time of recording equipment) and noise level as a measure of the resolution. The single crystal, dimensions 1 mm x 1 mm x 2 mm was oriented such that the cubic crystal axis coincided with those of the right angle scattering system. The results for this sample are also given in Table 2. The resolution here was poor with a signal to noise ratio of about 3 at maximum signal level, which may be attributed to the increased total absorption in the thicker sample.

An attempt was also made to measure the Raman spectra at 77°K by cooling the samples in liquid nitrogen. It was found however that a signal could not be detected due to the increased scattering of the laser light by the sample supports, dewar windows and bubbles in the liquid nitrogen.

Infrared absorption and reflection work has been previously carried out by Pastrnyak (1959), Bouster et al (1963), O'Keefe (1963), Heltemes (1966) and Carabatos (1967) but since there may be some disagreement due to differences in sample composition, it was felt that some infrared absorption curves should be included for completeness.

These were made on an unsupported film of Cu_2O ,

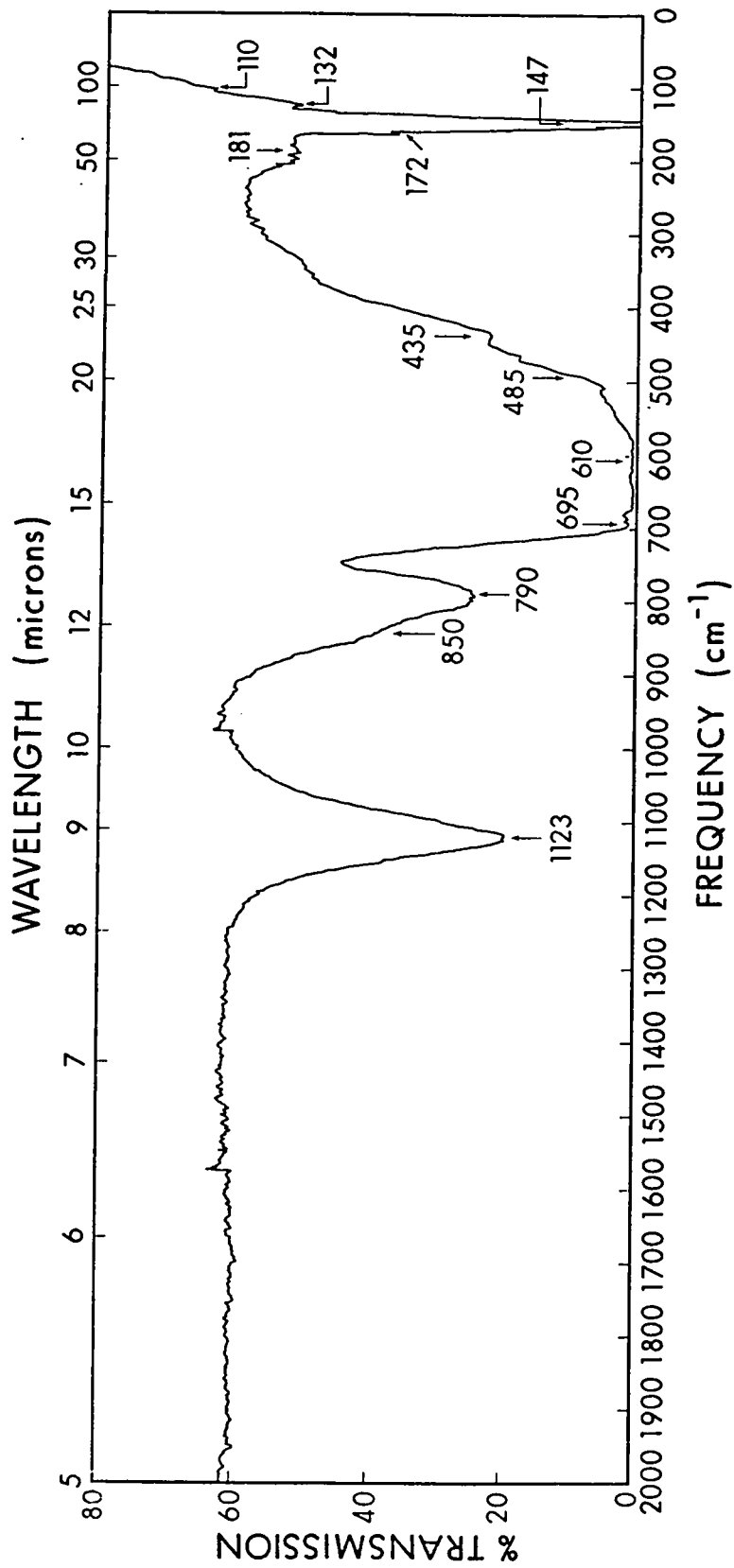
thickness 50μ , which was produced by grinding and etching a larger sample which had been grown under similar conditions to that on which the Raman scattering was measured. The frequency range $100 - 2000 \text{ cm}^{-1}$ was covered using a Perkin Elmer infrared spectrometer model 421 for the region $600 - 2000 \text{ cm}^{-1}$ and a second infrared spectrometer, Beckman IR11, in the range $100 - 600 \text{ cm}^{-1}$. The combined absorption curves are shown in Fig. 30.

The Raman and infrared absorption results are summarised in Table 2 together with previously reported data of the above authors.

Discussion

Cuprous Oxide has space group O_n^4 ($\cong Pn3m$) and group theoretical treatments on the phonon symmetries have been carried out by Elliott (1961) and Huang (1963). Two first order infrared active modes were found (symmetry $F_{1u} \cong \Gamma_{15}$) and were assigned to the strong infrared absorption bands at 610 and 147 cm^{-1} (Fig.30). The remainder of the absorption spectrum therefore has been assumed to be due to two phonon processes as shown in Table 3 with the exception of the strong absorption band at 1120 cm^{-1} . Pastrnyak (1959) has pointed out that the energy of this band corresponds closely to the

Figure 30 : Infrared transmission curve
for Cu_2O . Temperature is 297°K .



spin-orbit splitting of the valence band (0.13 eV) and hence to the energy difference between the two sets of exciton levels associated with this valence band and the first conduction band (the well known "yellow" and "green" series. Baumeister (1961) Elliott (1957), Nikitine (1955)). Since most spectrometers for infrared work, including those used here, illuminate the sample with white light and subsequently scan the transmitted spectrum, it is just possible that the 1120 cm^{-1} band is related to the exciton states since the visible light, which is incident on the sample at the same time as the infrared, could create the necessary excitons.

The process envisaged here would be one in which, for example, an $n=2$ exciton of the yellow series could be transferred to an $n=2$ of the green series by absorption of an infrared quantum.

A second possible explanation for the presence of the 1120 cm^{-1} band has been discussed by Carabatos et al (1968) who suggest that this absorption is due to impurities such as silicon in the Cu_2O lattice.

In our view, neither of these explanations is completely satisfactory since no definite experimental

correlations between the presence of excitons or impurities and the intensity of the absorption band have been made.

The 181 cm^{-1} phonon, which appears as a weak absorption band at this frequency, and also in phonon combination bands (see Table 3) has been assigned by Pastrnyak (1959) and O'Keefe (1963) to be a Raman active phonon.

In the group theoretical work by Huang (1963) and Carabatos (1968) only one phonon is found to be Raman active (symmetry $F_{2g} \equiv \Gamma'_{25}$). Huang (1963) tentatively predicted that this phonon should appear at 606 cm^{-1} while Carabatos (1968) has indicated that it should appear in the range $589 - 626 \text{ cm}^{-1}$.

It is therefore seen that there is some discrepancy between the infrared and group theoretical predictions as to the frequency of the Raman active phonon although no pronounced structure appears at either 606 or 181 cm^{-1} in the Raman spectrum (Fig. 29).

For a right angle scattering system, with the plane of polarisation of the incident light perpendicular to the plane of scattering, the depolarisation ratio for the F_{2g} vibrations of the O_h group should be $\rho = \infty$, independent of crystal

Table 3 : Known combination bands in
infrared absorption (see for example Pastrnyak (1959)).

Frequency	Combination	v'
850 (± 5)	662 + v'	188 (± 7)
790 (± 5)	610 + v'	180 (± 20)
485 (± 5)	662 - v'	177 (± 7)
429	610 - v'	181 (± 20)

orientation (Saksena (1940), Loudon (1964)).

The spectra obtained from a crushed sample are therefore valid in a determination of the Raman frequency. None of the measured Raman lines however corresponds to $\rho=\infty$; the highest value for ρ observed being 2.4, for a continuum part of the spectrum.

It is possible that multiple internal reflections in the samples (dielectric constant $\epsilon \approx 7$) have reduced the observed value of ρ from the theoretical value and that the strong line at 220 cm^{-1} corresponds to the Raman active phonon, although it seems improbable that these effects could reduce the depolarisation ratio to $\rho < 1$. A positive identification of the F_{2g} phonon can therefore not be made from the results given here.

It is interesting to note that some of the weak Raman lines correspond closely to absorption bands observed in the infrared, particularly the Raman lines at 485, 420 and 150 cm^{-1} (see Table 2). Further, the line at 106 cm^{-1} corresponds closely to the well known 105 cm^{-1} phonon responsible for the indirect transition steps appearing on the absorption edge of the material. This phonon, symmetry $E_u (= \Gamma_{12}')$ (Elliott (1961)) has not been

observed in the infrared absorption.

Infrared active phonons should not, of course, also be Raman active in Cu_2O but these strong correlations suggest that perhaps in a material such as Cu_2O , which has a large number of lattice defects (voids, inclusions, vacancies, vacancy clusters and surface impurities) local inversion symmetry may be lacking in parts of the crystal and the selection rule may break down.

It is more probable however that these Raman lines appear quite validly in the second order - two phonon processes. The bands at 485 and 420 cm^{-1} in particular have already been assigned in the infrared work as two-phonon combination bands (Table 3). The spectrum of Fig.29 is in fact second order continuous in character with fine structure, reflecting structure in the two-phonon density of states (Loudon (1964), Johnson and Loudon (1965)). A complete phonon scheme for the whole Brillouin zone has not been calculated for Cu_2O , however, which makes further analysis in this direction difficult.

Conclusion

The spectra presented above, although weak, are nevertheless of sufficiently good resolution to

allow a reliable determination of the depolarisation ratios. From these it seems unlikely that the first order Raman line has been observed although multiple internal reflections are possible in our samples which may influence the measured depolarisation ratios.

The use of a longer wavelength laser line having better light transmission should produce better resolution of the Raman spectrum and hopefully permit the F_{2g} phonon to be finally located.

APPENDIX A.

The Photon-Electron Interaction.

The Hamiltonian of a solid may be written

$$H_0 = H_e + H_L + H_{eL} \quad 16)$$

where H_e involves the electronic co-ordinates, H_L involves the lattice co-ordinates, and H_{eL} represents the electron-lattice interaction involving both electronic and lattice (ionic) co-ordinates. With the presence of a radiation field there are in addition the terms H_R , involving field co-ordinates, and H_{eR} and H_{LR} representing the interaction of the field with the electrons and lattice respectively.

For the radiation field frequencies we are concerned with in this thesis, we may neglect the lattice-field interactions (Reststrahlen). The Hamiltonian then becomes

$$H = H_0 + H_R + H_{eR} \quad 17)$$

In the usual semi-classical approach, the solid is treated quantum mechanically with H_0 as the

unperturbed Hamiltonian and H_{eR} as a perturbation. The solution of this problem gives the response of the solid to a given radiation field but does not give the properties of the radiation field itself in the solid (these may however be obtained from the classical Maxwell equations).

The electron-field interaction H_{eR} is given by the operator

$$H_{eR} = \sum_i \left[\frac{e}{mc} \underline{p}_i \cdot \underline{A}(\underline{r}_i) + \frac{jeh}{2mc} \nabla \cdot \underline{A}(\underline{r}_i) + \frac{e^2}{2mc^2} \underline{A}^2(\underline{r}_i) \right] \quad (18)$$

where \underline{r}_i are the electronic co-ordinates, \underline{p}_i is the momentum of the i^{th} electron and $\underline{A}(\underline{r}_i)$ is the vector potential of the radiation field. (Note : expression 18) has been derived from the classical Hamiltonian for a charged particle in an electro-magnetic field,

$$H' = \frac{1}{2m} \left(\underline{p} + \frac{e}{c} \underline{A} \right)^2.$$

The term $\nabla \cdot \underline{A}(\underline{r}_i)$ in expression 18) is zero for transverse radiation (the Coulomb gauge) and we neglect terms in \underline{A}^2 . The interaction Hamiltonian is therefore given by

$$H_{eR} = \sum_i \frac{e}{mc} \underline{p}_i \cdot \underline{A}(\underline{r}_i) \quad (19)$$

The vector potential for a photon field is of the form

$$\underline{A}(\underline{r}_i) \propto \underline{\varepsilon} e^{j\underline{k}' \cdot \underline{r}_i} \quad 20)$$

where $\underline{\varepsilon}$ is a unit vector in the direction of polarisation of the photon and \underline{k}' is the propagation vector.

Expanding $e^{j\underline{k}' \cdot \underline{r}_i}$ we have

$$\underline{p} e^{j\underline{k}' \cdot \underline{r}_i} \approx \underline{p} + j\underline{p}(\underline{k}' \cdot \underline{r}_i) \quad 21)$$

and the interaction Hamiltonian becomes

$$H_{eR} \propto \sum_i \{ \underline{\varepsilon} \cdot \underline{p}_i + j(\underline{\varepsilon} \cdot \underline{p}_i)(\underline{k}' \cdot \underline{r}_i) \} \quad 22)$$

The first term of 22) gives rise to the electric dipole interaction with electronic transition probabilities proportional to

$$|\langle 0 | \underline{\varepsilon} \cdot \underline{p} | f \rangle|^2 \quad 23)$$

where $|0\rangle$ and $|f\rangle$ are the initial and final electron states respectively. The second term of 22) gives rise to the electric quadrupole interactions which are important for direct transitions to the weak $n=1$ exciton of the yellow series as mentioned in the text.

We do not attempt here to give a complete treatment of the electron-photon interaction, but we shall discuss the relevant results and their implications. For a more detailed analysis, we refer the reader to the work by Elliott (1957, 1960, 1961), Knox (1963), Fan (1967), and Di Bartolo (1968).

For a solid, the states $|0\rangle$ and $|f\rangle$ will be made up of the electronic Bloch functions for the periodic lattice. For the case of weak electron-hole interactions, the exciton states associated with a valence band $|0\rangle$ and conduction band $|f\rangle$, can also be described in terms of the Bloch functions for the band extrema.

The transition probability for direct transitions to exciton states is proportional to

$$|\langle 0 | \underline{e} \cdot \underline{p} | \underline{k}, n \rangle|^2 \delta(E_0 - E_{\underline{k}, n} + h\nu) \rho(\nu) \quad (24)$$

where K is the exciton wavevector and n is the exciton band quantum number (from a Rydberg relation). The δ function describes the energy conservation requirement, $h\nu$ is the photon energy and $\rho(\nu)$ is the density of incident radiation of frequency ν .

Because the photon momenta are small compared to the scale of electronic momenta in the lattice

($k_e/k' \sim 10^3$), the momentum conservation condition is

$$\underline{k}_e + \underline{k}_h = 0 \quad (25)$$

where \underline{k}_e and \underline{k}_h are the wavevectors of the electron and hole respectively which make up the exciton state. The wavevector \underline{K} for the exciton is related to these by the relation

$$\underline{K} = \underline{k}_e + \underline{k}_h \quad (26)$$

and so for direct transitions we must have $\underline{K} = 0$, and we therefore observe a line spectrum in absorption due to transitions to a set of exciton bands $n=1,2,3..etc.$ with absorption coefficient α proportional to

$$|\langle 0 | \underline{\epsilon} \cdot \underline{p} | 0, n \rangle|^2 S_n(E) \quad (27)$$

where S_n is the density of states $|0, n\rangle$ per unit energy range at energy E .

We now distinguish the two cases a) "allowed" and b) "forbidden" transitions which correspond to transitions between states of opposite parity and states of the same parity respectively (the Laporte rule).

For allowed transitions the matrix elements in

27) are non zero, and the absorption coefficient can be calculated directly. For forbidden transitions however, it is found (Elliott(1957)) that the absorption coefficient should be proportional to

$$\frac{n^2 - 1}{n^5} \quad 28)$$

and a line spectrum should again be observed, only now there should be no absorption at $n=1$ (electric dipole only). This result corresponds closely to measurements of absorption in Cu_2O where the valence and first conduction band extrema both have even parity.

Thus far we have neglected the effects of lattice phonons, but for the case we have just discussed where electric dipole transitions to exciton states are forbidden and are strictly forbidden for the $n=1$ exciton level, we would expect that indirect transitions involving the absorption or emission of a lattice phonon would be important.

The expression for the absorption coefficient due to transitions to exciton states $|n, \underline{k}\rangle$ for this type of process contains the following product of matrix elements

$$\langle 0 | \underline{\epsilon} \cdot \underline{p} | i \rangle \langle i | H_{eL} | n, \underline{k}, n_{\underline{k}} \pm 1 \rangle \quad 29)$$

where the initial state of the crystal is denoted $|0\rangle$, $|i\rangle$ is some intermediate state of the system and $|n, \underline{k}, n_{\underline{k}} \pm 1\rangle$ describes the final state where an exciton in the n^{th} level is created with wavevector \underline{k} . The quantity $n_{\underline{k}}$ is the initial number of phonons of wavevector \underline{k} which are active in the electron lattice interaction H_{eL} . We note that for the process $|0\rangle \rightarrow |n, \underline{k}, n_{\underline{k}} \pm 1\rangle$ only the overall energy must be conserved.

For the case of Cu_2O , the valence and conduction band minima are both at $\underline{k} = 0$, and as has been discussed in the text, it was shown by Elliott (1960) that the steps appearing on the absorption edge were due to indirect transitions to the $n=1$ exciton level of the yellow series. The transitions giving rise to these steps involve the absorption or emission of a 105 cm^{-1} optical phonon with wavevector $\underline{k} = 0$. We have assumed the phonon dispersion curve near $\underline{k} = 0$ to be flat for the calculation of ϕ vs. $h\nu_i$ given earlier, and in fact this condition is also necessary to produce the strong background continuum in absorption (previously denoted α_1).

APPENDIX B.

A.P.L. Programs and Routines.

"DATA" : This routine contains the absorption information for α_1 and α_2 as a function of wavelength λ . The data is entered in groups of three numbers, the first being α_1 , the second α_2 , and the third λ . Both α_1 and α_2 are in cm^{-1} and λ is in Angstroms.

"DATAL 3" : This routine contains the luminescence intensity versus incident wavelength information for various sample thicknesses. Only the luminescence intensities corresponding to the same wavelengths as used in DATA are given (in arbitrary units).

"FNC 3" : This program computes the quantity $S' - S$ for a particular sample thickness and ratio $w_2:w_{21}$ (the quantity R if $x[4] = 1$).

"ITERATE" : ITERATE repetitively solves FNC 3 for $S' - S = 0$ and hence determines the quantity R for the particular sample thickness where S' is smooth.


```

VDATA[ ]V
V R+DATA
[1] R+ 6 0 6190 6.5 0 6180 7 0 6173 8 0 6155 10 0 6117 10.5 0 6103 12.5 0 6100
[2] R+R, 15 0 6095 20 0 6084 25 0 6070 30 0 6045 35 0 6025 45 0 5990 55 0 5962
[3] R+R, 60 0 5940 80 0 5900 100 0 5865 120 0 5835 140 30 5807 150 150 5795
[4] R+R, 170 20 5781 200 0 5735 250 0 5685 300 0 5640 350 0 5600 420 0 5570 500 0 5540
[5] R+((pR)÷3),3)pR
V

```

```

VDATAL3[ ]V
V R+DATAL3;A;B;C;D;E
[1] A+ 0 4 9 15 21 24 40 57 59 65 70 71 70 69 67 65 65 69 73 75 73 78
[2] A+A, 78 77 76 75 78
[3] B+ 0 3 7 11 16 18 50 63 69 79 87 89 88 85 82 77 74 75 78 80 75 70 63
[4] B+B, 57 50 44 44
[5] C+ 0 2 7 10 15 18 40 50 54 60 65 65 66 64 62 60 61 64 67 65 68 66 64
[6] C+C, 61 60 59
[7] D+ 0 3 12 18 30 32 40 55 65 80 86 89 88 84 82 80 78 81 82 82 82 76 69 64 59 53 52
[8] E+ 0 2 7 15 24 27 31 40 45 45 40 32 27 18 15 10 8 8 7 4 6 3 1 1 0 0 0
[9] R+Q(5,(pA)φA,B,C,D,E)
V

```

```

VFNC3[ ]V
V Q+R FNC3 X;A;B;C;D;E
[1] A+(1--X[3]×X[1])
[2] B+(X[1]+3×X[2]×X[4]÷(X[4]+R))÷X[1]+X[2]
[3] C+1--X[3]×(X[1]+X[2])
[4] Q+B×C
[5] Q+--(Q-A)
V

```

```

V ITERATE[ ] V
V R←N ITERATE X;A;B;C;D;E;Q
FNC3NUMBER←N
A←10*15-130
B←15
C←D+E←1
R←A[B]
SIGFIG←5
→(1000<N←N+1)/27
Q←R FNC3 X
→(Q=0)/0
→(Q>0)/20
→(E=0)/15
R←A[B+B-1]
→(B<2)/29
→7
R←R+A[B]
→(D=0)/7
D←0
C←B
→7
R←R+A[B+B+1]-A[B]
→(B≥ρA)/29
→(E=0)/24
E←0
→(D≠0)/7
→(B<C+SIGFIG)/7
→0
'ERROR RESULT = ;R;'1000 ITERATIONS'
→0
'ERROR RESULT = ;R;'ITERATION VECTOR GONE'
V

```

- [1]
- [2]
- [3]
- [4]
- [5]
- [6]
- [7]
- [8]
- [9]
- [10]
- [11]
- [12]
- [13]
- [14]
- [15]
- [16]
- [17]
- [18]
- [19]
- [20]
- [21]
- [22]
- [23]
- [24]
- [25]
- [26]
- [27]
- [28]
- [29]

"XSEC 3" : This program calculates the capture cross-sections ϕ as a function of wavelength using known luminescence data from a DATAL type of routine.

```

VXSEC3[ ]V
V P+XSEC3 X;A;R;R1;R2;L;S
  R+DATA
  [1] R1+R[;1]
  [2] R2+R[;2]
  [3] L+DATA L3[;X[1]]
  [4] S+L*(R1+R2-X[3])÷((*-X[3]*X[2])-(*(-(R1+R2)*X[2]))
  [5] P+S÷(R1+R2)
  [6] P+Q(2,(pP))pP,R[;3]
  [7]
V

```

BIBLIOGRAPHY.

- Di Bartolo, B. (1968) in "Optical Interactions in Solids" (Wiley and Sons Inc., New York)
- Baumeister, P.W. (1961) Phys. Rev. 124, 340.
- Bloem, J., Van der Houwer van Oordt, A.J., and Kroger, F.A. (1956) Physica 22, 1254.
- Bloem, J. (1958) Philips Research Reports 13, 167.
- Bouster, C., Claudel, J., Gerbaux, X. and Hadni, A. (1963) Ann. Phys. 8, 299.
- Carabatos, C. (1967) J. de Physique 28, 825.
- Carabatos, C., Diffine, A. and Sieskind, M. (1968) J. de Physique 29, 529.
- Carabatos, C. (1968) in "Colloque sur les Propriétés Physiques de la Cuprite", Strasbourg, France (Unpublished).
- Dahl, J.P. and Switendick, A.C. (1966) J. Phys. Chem. Solids 27, 931.
- Dahl, J.P., Brahms, S. and Nikitine, S. (1966) Phys. Letters 22, 31.
- Dyson, F.J. (1955) Phys. Rev. 98, 349.
- Elliott, R.J. (1957) Phys. Rev. 108, 1384.
- Elliott, R.J. (1960) in "Proceedings of the International Conference on Semiconductor Physics", Prague (Academic Press Inc., New York).

- Elliott, R.J. (1961) Phys. Rev. 124, 340.
- England, T.S. and Schneider, E.E. (1951) Physica 17, 221.
- Fan, Y.H. (1967) in Handbuch der Physik Volume XXV/2a
"Light and Matter Ia" (Springer-Verlag, Berlin).
- Feher, G. and Kip, A.F. (1955) Phys. Rev. 98, 337.
- Fortin, E. and Weichman, F.L. (1962) Can. J. Phys.
40, 1703.
- Fortin, E. (1965) Ph.D. Thesis.
- Frerichs, R. and Lieberman, I. (1961) Phys. Rev. 121, 991.
- Goldberg, P. (1966) in "Luminescence in Inorganic
Solids" (Academic Press Inc., New York).
- Gorban, I.S., Gritsenko, Y.I. and Rud'ko, S.N. (1961)
Fiz. Tverd. Tela 3, 2147 (see Soviet
Physics - Solid State 3, 1559 (1962)).
- Grillot, E. (1956) Acta. Phys. Hungar. 5, 445.
- Gross, E.F. and Kriengold, F.I. (1968) Zh. Eksper.
Teor. Fiz. Pis'ma 7, 281. (see JETP Letters
7, 218 (1968))
- Gross, E.F. and Pastrnyak, I (1959) Fiz. Tverd. Tela 1,
162 (see Soviet Physics - Solid State 1, 143
(1959)).
- Grun, J.B. (1962) Ph.D. Thesis.
- Grun, J.B. and Nikitine, S. (1962) J. Phys. 24, 355.
- Heltemes, E.C. (1966) Phys. Rev. 141, 803.
- Huang, K. (1963) Zeits. Phys. 171, 213.

- Johnson, F.A. and Loudon, R. (1964) *Proc. Roy. Soc.* A281, 274.
- Kallmann, H.P. and Spruch, G.M. (1962) in "Luminescence of Organic and Inorganic Materials" (Wiley and Sons, New York).
- Karkhanin, Y.I. and Vorob'ev, Y.V. (1961) *Fiz. Tverd. Tela* 3, 206.
- Karkhanin, Y.I. and Vorob'ev, Y.V. (1962) *Fiz. Tverd. Tela* 4, 3336 (see *Soviet Physics - Solid State* 4, 2442 (1963)).
- Knox, R.S. (1963) in *Solid State Physics, Supplement 5, "Theory of Excitons"* (Academic Press Inc., New York).
- Kuzel, R., Cann, C.D., Sheinin, S.S. and Weichman, F.L. (in Press) *Can. J. Phys.*
- Lashkarev, V.E. and Kossonogova, K.M. (1946) *Compt. Rend. Akad. Sci.* 54, 125.
- Loudon, R. (1964) *Advan Phys.* 13, 423.
- Nikitine, S. (1955) *J. Phys. Radium* 16, 40.
- Nikitine, S. (1959) *Phys. Chem. Solids* 8, 190.
- Nikitine, S., Reiss, R. and Perny, G. (1955) *Comptes Rend.* 240, 64.
- O'Keefe, M. (1963) *J. Chem. Phys.* 39, 1789.
- O'Keefe, M., Ebisuzaki, Y. and Moore, W.J. (1963) *J. Phys. Soc. Japan* 18, 131.

- Pastrnyak, I. (1959) Opt. i. Spectrosk. 6, 107 (see
Opt. Spectry. 6, 64 (1959)).
- Pastrnyak, I. (1961) Czech. J. Phys. 11, 452.
- Portis, A.M., Kip, A.F., Kittel, C. and Brattain, W.H.
(1953) Phys. Rev. 90, 988.
- Pringsheim, P. (1949) in "Fluorescence and
Phosphorescence" (Interscience Inc., New York).
- Saksena, B.D. (1940) Proc. Indian Acad. Sci. A11, 229.
- Seibt, M. (1939) Verh. Deut. Ges. 20, No.2.
- Taylor, J.C.W. and Weichman, F.L. (1969) Phys. Rev.
185, 1214.
- Tolstoi, N.A. (1957) Opt. i. Spektrosk. 2, 210.
- Tolstoi, N.A. and Abramov, A.P. (1967) Fiz. Tverd.
Tela 9, 3340 (see Soviet Physics - Solid
State 9, (1968)).
- Toth, R.s., Kilkson, R. and Trivich, D. (1960) J. Appl.
Phys. 31, 1117.
- Weichman, F.L. (1960) Phys. Rev. 117, 998.
- Weichman, F.L. and Kuzel, R. (1970) Can. J. Phys.
- Zhilich, A.G. and Makarov, V.P. (1961) Fiz. Tverd.
Tela 3, 585 (see Soviet Physics - Solid
State 3, 429 (1961)).
- Zielinger, J.P., Weichman, F.L., Zouaghi, M. and
Fortin, E. (1968) Rev. Phys. Appliquée 3, 140.